Report No. UT-26.15

DEVELOPMENT AND VALIDATION OF A METHODOLOGY TO ESTIMATE RETROREFLECTIVITY OF PAVEMENT MARKINGS USING LIDAR

Prepared For:

Utah Department of Transportation
Research & Innovation Division

Final Report
December 2025

RESEARCH
UDOT Keeping Utah Moving
Utah Department of Transportation - Research Division
4501 South 2700 West - P.O. Box 148410 - SLC,UT 84114-8410

DISCLAIMER

The authors are responsible for preparing and accurately interpreting the information, data, analysis, discussions, recommendations, and conclusions presented herein. The contents do not necessarily reflect the views, opinions, endorsements, or policies of the Utah Department of Transportation or the U.S. Department of Transportation. The Utah Department of Transportation makes no representation or warranty of any kind, and assumes no liability therefore.

ACKNOWLEDGMENTS

The authors acknowledge the Utah Department of Transportation (UDOT) for funding this research, and the following individuals from UDOT for participating on the Technical Advisory Committee and for helping to guide the efforts:

- Abdul Wakil
- David Stevens
- Ryan Ferrin
- Shawn Lambert
- Chris Whipple
- Benjamin Maughan
- Ethan Turner
- Dave Thomas
- Marc Sutton
- Brad Loveless
- Robert Miles
- Megan Leonard
- Jason Peterson
- Kevin Nichol
- Cooper Crystal
- Matt Luker
- Kendall Draney
- Radhakrishnan Ukkiramapandian
- Jeff Ericson

TECHNICAL REPORT ABSTRACT

1. Report No. UT-26.15	2. Government Accession No. N/A	3. Recipient's Catalog No. N/A
4. Title and Subtitle Development and Validation of a Methodology to Estimate Retroreflectivity of Pavement Markings Using LiDAR		5. Report Date December 2025 6. Performing Organization Code N/A
7. Author(s) Abbas Mohammadi, Juan Medina, Abbas Rashidi		8. Performing Organization Report No. N/A
9. Performing Organization Name and Address University of Utah Department of Civil and Environmental Engineering 110 S. Central Campus Drive, Suite 2000 Salt Lake City, UT 84112		10. Work Unit No. 5H094 32H 11. Contract or Grant No. 24-8331
12. Sponsoring Agency Name and Address Utah Department of Transportation 4501 South 2700 West P.O. Box 148410 Salt Lake City, UT 84114-8410		13. Type of Report & Period Covered Final Report Sep 2023 to Dec 2025 14. Sponsoring Agency Code PIC No. UT23.207

15. Supplementary Notes

Complementary work related to this project is sponsored by the Center for Transformative Infrastructure Preservation and Sustainability (CTIPS) University Transportation Center, supported by the Federal Highway Administration.

16. Abstract

Longitudinal pavement markings significantly affect traffic safety, particularly in adverse weather and nighttime conditions when crashes and fatalities are often overrepresented. Given the wide range of factors affecting the performance of pavement markings, periodic monitoring is needed to ensure their integrity and adequate retroreflectivity levels. Typical monitoring methods include individual readings from manual retroreflectometers and mobile setups where much larger segments can be covered in shorter periods. However, mobile setups require specialized equipment, calibration, and significant economic resources. This research uses LiDAR data collected as part of asset management efforts to help assess durable pavement markings, primarily longitudinal freeway lines. This project developed a framework to identify and isolate pavement markings from LiDAR point clouds, to filter and refine data, and to produce models and evaluate the associations between field-measured retroreflectivity and a combination of intensity from LiDAR readings, RGB data, and marking material. Freeway data was used to analyze the potential of LiDAR in assessing the retroreflectivity of pavement markings. Results show that LiDAR data can produce reliable associations to retroreflectivity levels both in terms of classification and value prediction to make maintenance decisions. A key component in the proposed methodology for prediction and classification is the clustering of individual assessments spatially correlated to produce robust segment-level outcomes. This study is complemented by a computer tool that implements the analysis methods and allows for processing of new datasets. In addition, a related project extends the work presented here to incorporate imagery into the analysis for more comprehensive assessments.

17. Key Words		18. Distribution Statement		23. Registrant's Seal
Pavement marking retroreflectivity, LiDAR intensity, machine learning, continuous and dashed lane line, reflective longitudinal roadway treatment.		Not restricted. Available through: UDOT Research & Innovation Div. 4501 South 2700 West P.O. Box 148410 Salt Lake City, UT 84114-8410 www.udot.utah.gov/go/research		N/A
19. Security Classification (of this report) Unclassified	20. Security Classification (of this page) Unclassified	21. No. of Pages 77	22. Price N/A	

TABLE OF CONTENTS

LIST OF TABLES

LIST OF FIGURES

LIST OF ACRONYMS

ASTM	American Society for Testing and Materials
CSV	Comma-Separated Values
CTIPS	Center for Transformative Infrastructure Preservation and Sustainability
DBSCAN	Density-Based Spatial Clustering of Applications with Noise
DOT	Department of Transportation
DT	Decision Tree
EB	Eastbound
FHWA	Federal Highway Administration
HOV	High Occupancy Vehicle
IQR	Interquartile Range
LEL	Left Edge Line
LiDAR	Light Detection and Ranging
LL	Lane Line
MAD	Median Absolute Deviation
$mcd/m^2/lux$	Millicandelas per square meter per lux
MSE	Mean Squared Error
MUTCD	Manual on Uniform Traffic Control Devices
NB	Northbound
R^2	Coefficient of Determination (R-squared)
RANSAC	Random Sample Consensus
REL	Right Edge Line
RGB	Red, Green, Blue
RL	Retroreflected Luminance
RMSE	Root Mean Squared Error
SB	Southbound
SVM	Support Vector Machine
UDOT	Utah Department of Transportation
UTM	Universal Transverse Mercator
WB	Westbound
WGS 84	World Geodetic System 1984
XGBoost	Extreme Gradient Boosting

EXECUTIVE SUMMARY

The outcomes from this project are intended to provide a solution to address recent regulatory needs set forward by the Federal Highway Administration (FHWA) to establish baseline levels of reflectiveness that pavement markings must meet. Under the new regulation, public agencies, including Departments of Transportation (DOTs), are required to implement a method for maintaining minimum levels of retroreflectivity for markings, with compliance for such requirements expected to be in place by September 2026. Both the methodology and the computer tool generated from this project support this need and provide the basis for such federal reporting.

The proposed methodology obtains associations between field-measured pavement marking retroreflectivity and light intensity collected from LiDAR surveys. This scalable solution was devised to identify and isolate pavement markings from the LiDAR point cloud, perform data filtering, and fit models using traditional regression models and machine learning to generate accurate assessments and classification of retroreflectivity levels.

Among different models tested throughout this research, and compared to the best-performing traditional regression model with an exponential functional form, Extreme Gradient Boosting (XGBoost) models provided the strongest predictive capabilities. The models achieved correlation values (R^2) above 0.8 for the best-performing freeways, with low Root Mean Squared Error (RMSE) in the order of 20 to 30 mcd/m^2/lux. These results indicate a robust monotonic correlation between LiDAR intensity and retroreflectivity.

In addition, classification assessments were first obtained for individual points, and then refined through a hierarchical clustering approach that grouped road segments based on mileage and intensity. Such segmentation ensures that the predictive models are applied to cohesive sections of roadway, enhancing the evaluation of compliance with FHWA retroreflectivity standards. After testing different classification models, results from Random Forest classifiers achieved high performance metrics, with some lane markings reaching over 90% classification accuracy at the point-level, and up to 100% accuracy when 1-mile segment-level assessments were produced.

The proposed methodology has the potential to enable transportation agencies to prioritize maintenance efforts effectively, ensuring roadway safety and optimal resource allocation.

The analysis was focused on durable longitudinal pavement markings at different locations across the roadway sections, including the continuous right and left edge lines, as well as the dashed lane lines. However, extensions could also consider other roadway types, further reducing the need for extensive retroreflectivity surveys.

This study is complemented by a computer tool that implements the analysis methods and allows for the processing of new datasets. This tool is a portable solution that can be executed from any standard computer. The executable files and all dependencies were packaged for easy user access, discussed with the Technical Advisory Committee, and finalized in coordination with their recommendations. In addition, a separate but related project extends the work presented here to incorporate imagery into the analysis for more comprehensive and robust assessments aligned to the original objective of this project.

1.0 INTRODUCTION

Retroreflectivity of longitudinal pavement marking plays a significant role in communicating to drivers their location with respect to roadway lanes, particularly during low light and low visibility conditions (Carlson et al., 2009; National Safety Council, 2024). As such, retroreflectivity has a significant impact on traffic operations and safety (Ai & Hennessy, 2022; Chen & Fanny, 2019). Moreover, a recent ruling from FHWA introduced a mandate for transportation agencies to develop a process to maintain minimum levels of retroreflectivity on public roads, resulting in the need for agencies to measure and monitor pavement markings in order to maintain compliance with such requirements (Federal Highway Administration, 2022; Mousa, 2023).

Typically, retroreflectivity of pavement markings is measured using retroreflectometers operated manually or mounted on mobile devices. However, even though mobile setups allow for the collection of measurements at driving speeds, they require special equipment and represent high costs (Lee, 2016). Thus, in general, monitoring and maintaining the retroreflectivity of pavement markings, which is crucial for their effectiveness, are both labor-intensive and costly (Mahlberg et al., 2021). Therefore, improvements leading to retroreflectivity estimates without extensive data collection needs could represent a significant reduction in related costs and data processing.

This project targets an opportunity to achieve such benefits by repurposing LiDAR datasets the agency already collects periodically, and postprocessing them to extract retroreflectivity estimates intended to supplement and eventually replace field measurements using reflectometers. This project used existing datasets from previous LiDAR surveys to establish relationships and develop classification models to assess pavement marking retroreflectivity, and it is also producing a computer tool for the agency to obtain retroreflectivity assessments as new LiDAR data becomes available. The tool is currently being finalized through additional funding obtained from the CTIPS (Center for Transformative Infrastructure Preservation and Sustainability) university transportation center.

1.1 Objectives

The primary objective of this research is to develop a methodology that leverages existing mobile Light Detection and Ranging (LiDAR) data to assess the retroreflectivity of durable longitudinal pavement markings, particularly in light of new requirements from FHWA on establishing and implementing a method for maintaining minimum levels of retroreflectivity for markings.

This research aims to reduce the dependence on specialized equipment for measuring retroreflectivity and extensive labor, thereby cutting costs while improving the efficiency and coverage of retroreflectivity assessments. Additionally, this research seeks to support public agencies in meeting the upcoming FHWA standards by providing a reliable, scalable solution for maintaining pavement markings at the required levels of visibility.

This project is expected to provide a significant stepping stone toward developing a program to monitor pavement marking retroreflectivity, as recently mandated by new FHWA standards due for implementation by 2026.

1.2 Scope

This research involved a series of tasks evaluating the feasibility of using LiDAR data for retroreflectivity assessment. The key tasks included extracting relevant pavement marking data from extensive LiDAR datasets collected as part of routine asset management activities, developing and applying data postprocessing methods, and creating models to estimate retroreflectivity based on LiDAR intensity readings.

The study focused on integrating these methodologies with existing data collection frameworks to create a comprehensive pavement-marking management system that UDOT and similar agencies nationwide could use. The datasets used in this study consist mainly of durable longitudinal pavement markings on freeway segments; therefore, the models and findings are most directly applicable to durable marking materials rather than short-life paint treatments.

1.3 Outline of Report

This report describes the work performed as part of the research project, including the motivation and previous work in the area, a new methodology tailored to specific resources available to UDOT, the corresponding research questions, and a detailed depiction of results from the modeling and classification outcomes. Finally, the report summarizes the overall outcomes, implications, and recommendations for future work and implementation. More specifically, the report is structured in chapters as follows:

1. Introduction
2. Background
3. Data Collection
4. Data Analysis Methods
5. Modeling Results
6. Conclusions
7. Recommendations and Implementation

2.0 BACKGROUND

Despite few studies exploring the relationships between retroreflectivity of pavement markings and LiDAR data, there are still significant open questions on several fronts, including the selection and filtering of data from the LiDAR point cloud, models to best represent such relationships, the effects of treatment materials, external conditions, elapsed in-service time, and angle and distance of the intensity reading, among others. This chapter provides a description of previous efforts in this area.

2.1 Pavement Marking Retroreflectivity

The study of pavement marking retroreflectivity is crucial for understanding how well road markings can support driving tasks, particularly under challenging conditions such as nighttime driving or adverse weather. Retroreflectivity, as a measure of the amount of light reflected back to its source, is a crucial indicator of the visibility of these markings. Traditional methods of assessing retroreflectivity involve using handheld retroreflectometers or mobile setups following ASTM standards that require substantial resources, including time, labor, and equipment.

Numerous factors influence the retroreflectivity of pavement markings, including the infrastructure's condition, the marking placement quality, material type, and the maintenance practices employed (Mazzoni et al., 2024; Migletz & Graham, 2002). Over time, retroreflectivity tends to degrade due to exposure to traffic, weather, and other environmental and external conditions, with higher degradation rates at the beginning of the in-service life (Idris et al., 2024). For example, research indicates that some pavement markings can lose 33-40% of their initial retroreflectivity within the first year of service (Kirk et al., 2001; Migletz et al., 1999). Therefore, regular assessments are necessary to ensure the continued effectiveness of these markings, mainly to comply with safety standards set forth by agencies like the FHWA (Pike et al., 2022).

Traditional methods, such as nighttime inspections and retroreflectometers, are widely used to assess pavement marking retroreflectivity. However, these methods are often labor-intensive and costly, limiting their application over large areas. Recent advancements in mobile

LiDAR technology offer a promising alternative, particularly when these datasets are already being collected primarily to support other programs, such as roadway asset monitoring (Olsen et al., 2018). Roadway surveys from LiDAR systems often cover the complete paved area of cross sections, not only capturing location and geometric information of road markings, but also the intensity of the reflected laser light over the markings, which can be correlated with retroreflectivity values (Che et al., 2019).

2.2 LiDAR Technology in Road Asset Management

LiDAR, or Light Detection and Ranging, is a remote sensing technology that uses laser pulses to measure distances. It is increasingly used in road asset management because it generates high-resolution 3D maps of roadways and their surroundings (Mohammadi et al., 2025). The integration of LiDAR with pavement marking assessments represents a significant advancement in the field of transportation infrastructure management (Mohammadi et al., 2024).

In particular for this application, LiDAR data acquisition involves using vehicle sensors to scan the right of way as they travel along the road. The data collected includes spatial coordinates of road features, the intensity of the returned laser signals, and a distribution of red, green, and blue signatures (i.e., RGB parameters) received back at the sensor, all of which can provide insights into the reflective properties of pavement markings. A series of calibration processes must be undertaken to evaluate object reflectivity accurately using these intensity measurements, and the data is typically collected in .las or .laz formats and can be later converted into a wide range of formats as needed.

Previous researchers have taken steps toward the use of LiDAR for pavement marking identification and retroreflectivity estimation (Barçon et al., 2022). Guan et al. (2016) studied various methods for extracting road markings. They found that while many approaches are based on the geometric features of roads, some methods enhance accuracy by integrating additional data sources such as videos, maps, and aerial surveys to confirm the boundaries of the pavement.

The results of the LiDAR data collection process are typically projected onto a two-dimensional plane for analysis, applying detection thresholds to specify road markings (Yang et al., 2012). Due to the LiDAR angle of incidence, the accuracy can be affected by the varying distances between the sensor and the specific pavement marking being analyzed. To address this issue, researchers have adjusted the intensity values, considering both the distance and the angles to these more distant data points. Instead of modifying the recorded intensity values, some researchers have decided to use the threshold for detection, making it variable based on distances and angles (Kumar et al., 2014).

Hou et al. (2024) demonstrated using mobile LiDAR to locate and assess pavement markings by developing and evaluating new automated LiDAR processing algorithms. Additionally, their research investigated the feasibility of identifying the deterioration trend of retroreflectivity conditions. The study involved developing a comprehensive pavement marking inventory with retroreflectivity conditions for 14 selected testing sections and comparing historical and current data to determine deterioration trends for three marking materials: polyurea, epoxy, and thermoplastic.

Manasreh et al. (2024) focused on predicting retroreflectivity using the intensity of mobile LiDAR data, highlighting their correlation. The study provided a framework for pavement marking assessments using relatively inexpensive LiDAR sensors, showcasing the potential of machine learning techniques in this domain. The methodology included comprehensive feature extraction from LiDAR data, feature selection, and evaluation of various learning algorithms, achieving an R-squared of 0.824 on unseen data.

Lastly, He et al. (2023) introduced a vehicle-mounted LiDAR-based perception and evaluation method for retroreflection of road traffic markings, aiming to address the inefficiency in retroreflection maintenance. A calibration prediction model for LiDAR is established using a regression decision tree, enabling accurate prediction of road markings' retroreflected luminance (RL) values. A maintenance evaluation model was developed based on China's national standard, achieving an agreement of over 85% with traditional methods and reducing time costs by at least 90%. The study compared multiple linear regression functions, second-order polynomial functions, and decision trees for the calibration prediction model, with the decision tree showing the best fit (coefficient of determination = 0.95).

3.0 DATA COLLECTION

This chapter outlines the data collection process for this research, explaining the methods used to gather retroreflectivity and LiDAR data, the rationale behind these methods, and how lane markings are identified, ensuring accuracy and reliability. The detailed postprocessing of the LiDAR and retroreflectivity datasets plays a crucial role in the study, laying the foundation for the subsequent analysis and model development presented in the following chapters.

3.1 Retroreflectivity Data

Retroreflectivity data was collected prior to this project, and as part of efforts set in place by the state to monitor pavement marking performance on selected roadway segments. This data was taken from surveys conducted in the fall of 2023, serving as a baseline for evaluating the condition of pavement markings and for comparison to metrics derived from LiDAR data, also collected in the same time frame.

For the roadway sections included in this project, the monitored markings are predominantly durable longitudinal pavement markings (e.g., long-life materials installed on freeway mainline), which form the basis of the analyses and models presented in this report.

3.1.1 Data Collection Process

The retroreflectivity measurements were obtained using a mobile setup calibrated to follow ASTM standards for pavement marking assessments (Benz et al., 2009a). These standards ensure that the data collected represents the reflective properties of the markings as they would appear to drivers. Each measurement in the dataset corresponds to a specific location along the highway, identified by its section milepost and coordinates. The data includes the average and variance of retroreflectivity values for each location, as well as counts of valid and invalid measurements. Measurements were typically presented at intervals of 0.1 miles, ensuring detailed coverage along the roadway.

3.2 LiDAR Data

The LiDAR data was also collected prior to this project and primarily serves as a basis to support the monitoring of roadway assets. LiDAR data provides detailed spatial resolution of light reflection intensity, and thus, it was deemed suitable to support potential assessments about the performance of pavement markings.

3.2.1 Data Collection Process

LiDAR data was collected by a vendor that regularly surveys state-managed routes for the Utah Department of Transportation (UDOT). The data was initially provided in .las or .laz formats, which are standard for LiDAR but require conversion to more manageable formats for analysis. Using Python, the data was converted to CSV format, integrating it with the retroreflectivity data for comprehensive analysis. The processed LiDAR data includes X, Y, and Z coordinates, indicating the 3D spatial locations of points on the highway. Additionally, the data contains intensity values that reflect the strength of the laser beam return, as well as RGB values that help visualize the markings in a manner closer to how they appear in reality.

3.2.2 Data Alignment and Availability

Since the LiDAR data was collected in the UTM Zone 12 N coordinate system, it was converted to the WGS 84 system used by the retroreflectivity data. This conversion involved applying appropriate scale and offset values to ensure accuracy. The converted data, including the new latitude and longitude columns, allows for direct comparison and integration with the retroreflectivity measurements.

3.3 Postprocessing LiDAR and Retroreflectivity Data

The postprocessing phase is a critical step in this research, involving custom extraction of lane marking information from LiDAR datasets and integrating this data with on-ground retroreflectivity measurements. In addition, the postprocessing stages are also aimed at having a method that is as fully automated as possible, so the following steps have been incorporated into computer scripts that facilitate the processing of large datasets along extensive roadway sections.

It is important to mention that roadway construction and maintenance logs were reviewed to ensure that no new striping was installed on the sections included in this study between the dates the retroreflectivity and LiDAR datasets were collected, ensuring that the measurements were suitable for the analysis.

3.3.1 Locating Lane Markings Within LiDAR Cross-Sections

The first postprocessing task is accurately identifying the lane markings within the LiDAR data. This is accomplished by using the coordinates of the retroreflectivity measurements taken directly from the road, serving as a guide to identify a lane marking within the LiDAR cross-sections. A rectangular sampling area is first established within the LiDAR data, centered on the point where field retroreflectivity readings were located. This rectangle is sized to encompass all relevant data points around the lane marking, ensuring the markings are correctly located within the LiDAR dataset. This area is shown in Figure 3-1.

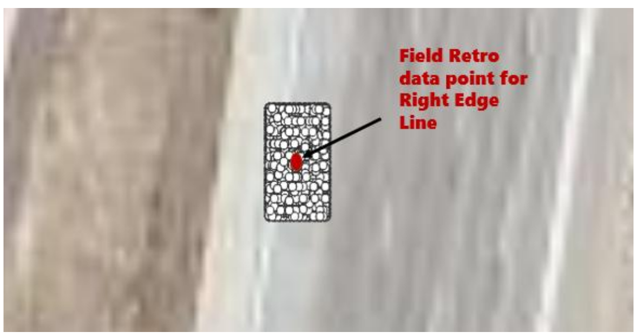

Figure 3-1 Sampling Area from LiDAR Data

3.3.2 Filtering Based on Intensity Values

Once the lane markings have been identified, the next step is to filter the data based on the intensity values recorded by the LiDAR sensor. The intensity of the LiDAR returns is crucial for distinguishing lane markings from the surrounding road surface. A detailed grid, with points spaced 0.2 feet apart, is constructed within the rectangular sampling area. This grid allows for a precise cross-sectional analysis of the LiDAR data at the location of the lane marking, which enhances the accuracy of the analysis. The filtering stage is a vital component of the postprocessing phase, where specific methods are used to isolate road lines within the LiDAR data (Cheng et al., 2020; Cheng et al., 2024). The steps in this process are as follows:

- Application of the RANSAC Algorithm: The RANSAC (Random Sample Consensus) algorithm is applied to the selected area to further refine the data. This technique aids in filtering out noise and irrelevant data points, concentrating only on those likely to represent the lane markings. This step significantly improved the accuracy of the analysis.

- Identification of High-Intensity Points: Within the sampling area, each point in the LiDAR data is represented as a dot, with an associated intensity value of the laser return. Higher-intensity points are prioritized, as they are most likely to correspond to the paint used in road markings over the darker, less reflective pavement surface. A sample image of the selection of high-intensity points, where darker shades identify the lane marking, is shown in Figure 3-2.

Figure 3-2 Filtering to Identify Lane Markings

- Extraction of Lane Markings: After filtering, the remaining high-intensity points are connected to form a line identified as the road marking. This line is added to the dataset of confirmed lane markings, creating a comprehensive map of the roadway's lane markings. The extracted lane marking from a sample rectangle is illustrated in Figure 3-3.

Figure 3-3 Extraction of the Lane Markings

3.3.3 Sequential Identification of Subsequent Sampling Areas

After processing one sampling area, the methodology proceeds by identifying the next sampling area. This systematic approach ensures that all roadway lane markings are captured, analyzed sequentially, and organized. By maintaining a structured process, this step-by-step progression minimizes the risk of missing critical sections of the roadway. The orientation and placement of the new sampling area are determined based on the lane markings identified in the previous steps.

This alignment ensures that the new sampling area is consistent with the actual direction of the road lines, as shown in Figure 3-4. By aligning the new sampling area with the direction of the lane marking in the current area, the process follows the roadway in both straight and curved segments. This alignment process is crucial for ensuring that the analysis remains consistent along the roadway, easing automation.

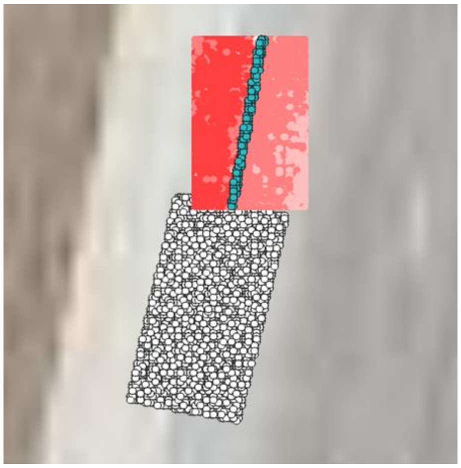

Figure 3-4 New Sampling Area

3.3.4 Verification of Continuous Lane Marking Presence

The final step in the postprocessing sequence involves verifying the continuous presence of lane markings within each sampling area. If the lane markings are consistently detected, the process continues to the next area, repeating the filtering and identification steps. However, if the markings are not consistently present, the process skips ahead to the next field-measured retroreflectivity point. The same data extraction and lane marking identification methods are applied for each new sampling area.

The process continues sequentially, aligning each new area based on the lane markings identified in the previous sections. This iterative approach ensures that all retroreflectivity measurements are thoroughly analyzed and that all lane markings on the roadway are accurately identified. The results of this iterative process are shown in Figure 3-5.

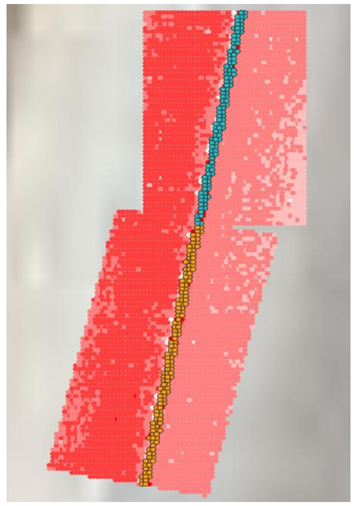

Figure 3-5 Next Sampling Area Analysis Result

4.0 DATA ANALYSIS METHODS

This chapter provides a detailed evaluation of the data collected and processed in the previous sections. It outlines the statistical methods employed, the rationale behind their selection, and the interpretation of the results obtained from various analyses.

4.1 Road Marking Extraction

This section presents examples demonstrating the effectiveness of our methods in identifying road markings from the LiDAR and retroreflectivity datasets. The result of road marking extraction for a small section of I-15 is shown in Figure 4-1. Figure 4-1a successfully identifies the road's right edge line. The clearly delineated right edge confirms the reliability of the filtering and extraction techniques. Figure 4-1b presents a more complex scenario, showcasing the left edge of the road, the HOV (High Occupancy Vehicle) lane, and the dashed lines between lanes. Despite the increased complexity, our method successfully distinguishes between different types of road markings:

- Right Edge Line (REL): The continuous white line along the right boundary of the road is accurately identified.
- Left Edge Line (LEL): The continuous yellow line along the left boundary of the road is accurately identified.
- HOV Lane: The designated lane for high occupancy vehicles is correctly differentiated from other lanes.
- Lane Lines (LL): The intermittent lane markings are clearly separated, demonstrating the method's capability to handle varied and discontinuous patterns.

(a) Extracted REL

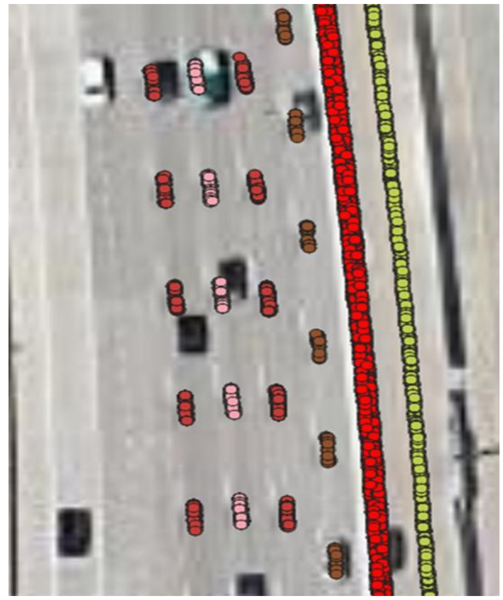

(b) Extracted Dashed Lines, HOV Line, and LEL

Figure 4-1 The Result of Road Marking Extraction

4.2 Outlier Identification

Different algorithms to identify and remove outliers were evaluated to reduce the incidence of unexpected readings in the modeling efforts (Golazad et al., 2024). It is recognized that outliers are also helpful to understand potential deficiencies and edge cases as a result of the data collection process, but they may also present difficulties for models to capture the overall relationship between field retroreflectivity and LiDAR intensity.

The following outlier identification methods were evaluated:

- Interquartile Range (IQR) Method: This method calculates the first quartile (Q1) and third quartile (Q3) and defines outliers as those outside the range [Q1 - 1.5IQR, Q3 + 1.5IQR], where IQR is the interquartile range.

- Z-Score Method: This method calculates Z-scores and defines outliers as those with a Z-score outside the range [-3, 3].

- DBSCAN (Density-Based Spatial Clustering of Applications with Noise): This method uses the DBSCAN clustering algorithm to identify outliers as noise points that do not belong to any cluster.

- Isolation Forest: This method uses the Isolation Forest algorithm to identify outliers as points with an outlier score below a certain threshold.

- Modified Z-Score Method: This method calculates the Modified Z-score for each' Ave' value using the median and median absolute deviation (MAD), defining outliers as those with a modified Z-score outside the range [-3.5, 3.5].

Each outlier removal method was applied to the datasets, and the results were analyzed to determine their effectiveness in terms of the correlation between retroreflectivity and average intensity, as well as the mean squared error (MSE).

Overall, the modified Z-score method was identified as the most favorable outlier detection algorithm and was consistently used for all datasets prior to developing trend models.

4.3 Normalization

As part of the data preprocessing, the average intensity values are normalized using Min-Max Scaling to bring all values into a range between 0 and 1 (Cheng et al., 2022). This normalization is essential for various data analysis and machine learning tasks, ensuring that the data is on a common scale without distorting differences in the ranges of values. The Min-Max Scaler is applied to the average intensity prior to being used as an independent variable to obtain an estimate of retroreflectivity.

4.4 Trend Modeling

A variety of functional forms were also evaluated in the process to characterize the relationship between LiDAR intensity and field-measured retroreflectivity. These models included both traditional regression-based models and machine learning methods, and ultimately resulted in the development of models for one traditional technique and one machine-learning algorithm, providing opportunities to compare both approaches. On one hand, the interpretability of traditional regression models is certainly an advantage to understand the relationship between inputs and outputs, compared to a more flexible, non-parametric approach with the machine learning alternatives.

The following were the models initially included in the exploration phase for the two categories, where *Y* refers to the retroreflectivity to be estimated as a function of the LiDAR intensity (*X*), constants *a*, *d*, and vectors of constants *b*, *c* for vector *X*.

4.4.1 Traditional Regression Models

- Linear Model: $Y = a + bX$
- Polynomial Model: $Y = a + bX + cX^2$
- Power Model: $Y = a * X^b$
- Exponential Model: $Y = a * \left(e^{(d+cX)}\right)$

4.4.2 Machine-Learning Models

- XGBoost (Extreme Gradient Boosting): This technique combines a supervised machine learning strategy with decision trees, ensemble learning, and gradient boosting. XGBoost has been a leading alternative for both regression and classification, and it was suitable for the analysis in this project.

The overall initial results from the regression efforts showed superiority of the exponential model and the XGBoost models, and were selected for the subsequent analysis and trend characterization.

Given the potential differences between specific lanes and highways, the decision was to investigate the relationship between retroreflectivity and LiDAR intensity separately for the right edge line, the left edge line, the HOV, and the dashed lines. Moreover, separate models were also produced for left edge lines where the cross section had a different number of lanes, and also for dashed lines based on their location with respect to the left-most lane.

4.5 Classification Modeling

In addition to the trend or regression modeling, efforts were also directed at developing a methodology to produce assessments of retroreflectivity based on LiDAR data. The main objective of the classification algorithms was to evaluate whether a roadway segment is expected to have retroreflectivity levels above or below a threshold. This approach is intended to produce outcomes to support decision-making when evaluating pavement markings in light of the new minimum retroreflectivity established by FHWA in the MUTCD. Thus, instead of producing retroreflectivity assessments, the classification outcomes are given as a binary decision with a determination of "above" or "below" a threshold, or "within" one of multiple categories.

The exploratory phase into the classification models identified alternative classification methods and ultimately led to a single approach to be applied to the final datasets.

The following classification models were considered in the process:

- Decision Trees (DT)
- Support Vector Machine (SVM)
- Random Forest

Models were trained and tested using the LiDAR intensity data and other relevant features. Then, a comparison of outcomes indicated that Random Forest provided the most favorable flexibility and stronger performance in handling binary classification tasks in our context.

It is noted that a key element in our methodology was to first identify clusters of data from consecutive road segments, to produce robust segment-level classification assessments based on multiple data points, as opposed to only producing an assessment for each individual point. The segments were determined by grouping (or clustering) data points with similar characteristics (e.g., LiDAR intensity levels, treatment material), making the classification process more effective in identifying patterns.

In this process, once the data were segmented, the Random Forest classifier was applied to generate point-level classifications, and these classifications were then aggregated within each segment to produce segment-level outcomes. The final results indicate whether entire segments, rather than just individual points, fall above or below the specified retroreflectivity threshold.

The outcomes from the classification models provide a clear indication of whether road segments meet a specified threshold, which in this context was set to be equal to the new minimum required retroreflectivity standards (Benz et al., 2009b).

Thus, by combining the classifications from all points within the same segment, the analysis yields more reliable segment-level assessments, ensuring that the overall quality of road markings is maintained. The segment-level approach is particularly useful for informing maintenance decisions and prioritizing areas that require immediate attention.

4.5.1 Clustering

The clustering process is a crucial step in analyzing the retroreflectivity of pavement markings, particularly for segment-level assessments. The methodology employed for clustering involved hierarchical clustering, combined with several refinement steps to ensure that the resulting clusters are meaningful and representative of actual road segments.

Before performing clustering, it is essential to standardize the data to ensure that all features contribute equally to the clustering process. The Chain (representing mileposts) and average LiDAR intensity were standardized using the StandardScaler function. This step transformed the data to have a mean of 0 and a standard deviation of 1, allowing for a balanced comparison between features during clustering.

The core of the clustering process utilized hierarchical clustering with Ward's method. Ward's method is well-suited for this analysis because it minimizes the variance within each cluster, leading to more compact and distinct clusters. The clustering begins by treating each data point as its own cluster, then iteratively merging clusters based on the smallest increase in total within-cluster variance. A distance threshold parameter was introduced to control the sensitivity of the clustering process, dictating how close data points must be to be grouped together. This threshold was adjusted iteratively to avoid overlaps between clusters.

To ensure the clusters reflected meaningful road segments, the initial clusters were reassigned based on the most frequent cluster within a defined mileage range (e.g., 3 miles). This step involved analyzing each data point's surrounding region and reassigning it to the cluster that was most common within that range. This reassignment helped align the clusters more closely with real-world road segments.

Small clusters that do not represent significant road segments were identified and merged with nearby clusters. This step was crucial to ensure that all clusters had a sufficient range and represented meaningful sections of the road. The threshold to preserve a cluster was ultimately set to 1 mile, so smaller clusters were merged with the nearest larger cluster based on the proximity in both mileage and intensity features.

After the initial clustering, reassignment, and merging, further refinement was necessary for points at the extreme ends of clusters (minimum and maximum mileage points). These extreme points were evaluated again for reassignment if they were closer in characteristics (e.g., intensity) to the neighboring cluster. This process increases the chances for clusters to align with actual road conditions.

Cluster overlaps were also evaluated as a verification step, so that eventual overlap scenarios were removed by adjusting the distance threshold parameter through iterations until all overlaps were resolved.

Once the datasets were clustered and refined, the next step involved implementing the Random Forest classifier to assess whether the retroreflectivity of pavement markings exceeded the selected threshold. The Random Forest classifier was trained using the scaled average LiDAR intensity, the scaled average LiDAR red color values (from the LiDAR RGB measurements), and the pavement marking material as the feature, where the material categories in this dataset correspond mainly to durable pavement markings used on UDOT freeways. In turn, the average category (i.e., above or below threshold) was obtained as the target. The model was evaluated using a training and testing split, with 80% of the data used for training and 20% for testing.

Finally, the model performance was assessed using typical classification metrics, including accuracy, precision, recall, and F1 score, providing a comprehensive evaluation of the model's effectiveness in predicting retroreflectivity compliance (Chen et al., 2024; Holzmann & Klar, 2024).

5.0 MODELING RESULTS

This chapter includes the outcomes from the modeling efforts to quantify the associations between retroreflectivity and LiDAR-related variables, both in terms of regression/trends models and classification models (Mohammadi et al.; Mohammadi et al.).

As described in the previous chapter, trend/regression modeling was conducted on the final datasets using a traditional regression technique with an exponential model form and also an XGBoost approach. In addition, classification models were completed using a random forest approach.

Results are first summarized to illustrate the original data before the outlier removal and scaling processes, followed by the trend/regression analysis, and lastly by the classification models. In all cases, individual lane markings were analyzed separately whenever possible for each of the freeways in this study.

5.1 Original Dataset Before Outlier Removal and Scaling

5.1.1 Right Edge Line

Figures 5-1 to 5-6 illustrate scatter plots comparing field-measured retroreflectivity with average LiDAR intensity values for the right-edge-line scenarios. These plots reveal a generally positive correlation between the LiDAR intensity and retroreflectivity, which is consistent with expectations.

Notably, the increase in retroreflectivity with higher LiDAR intensity appears to follow an accelerating trend, hinting at possible non-linear dynamics in their relationship. Additionally, distinct clusters can be observed within the plots, representing data points from road sections treated with different materials or with different in-service time (i.e., corresponding to different installation periods).

Figures 5-1 to 5-4 show individual models for three freeways (i.e., I-15, I-84, and I-80) and the two directions of travel, whereas Figures 5-5 and 5-6 show consolidated models for the two directions of travel for I-15 and I-84 only, where the datasets were more comprehensive and covered a wider range of values.

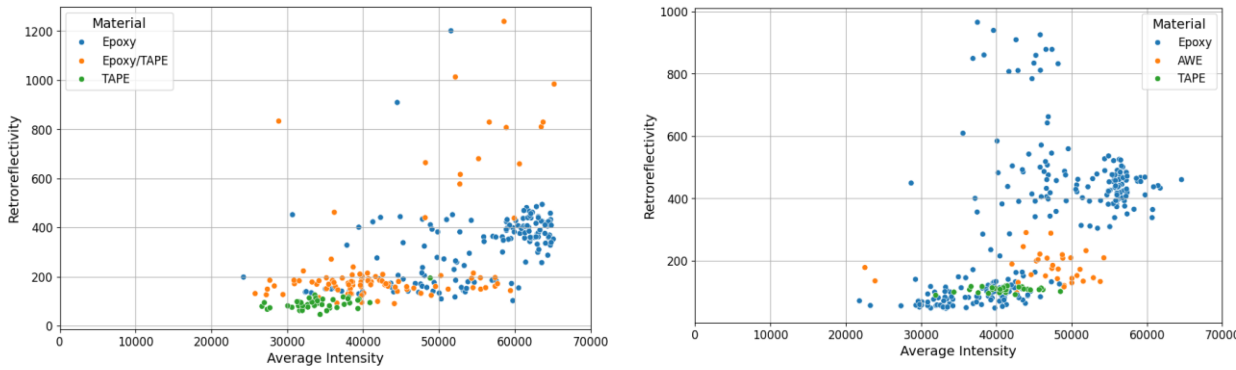

Figure 5-1 I-15 Right Edge Line: a) Northbound and b) Southbound

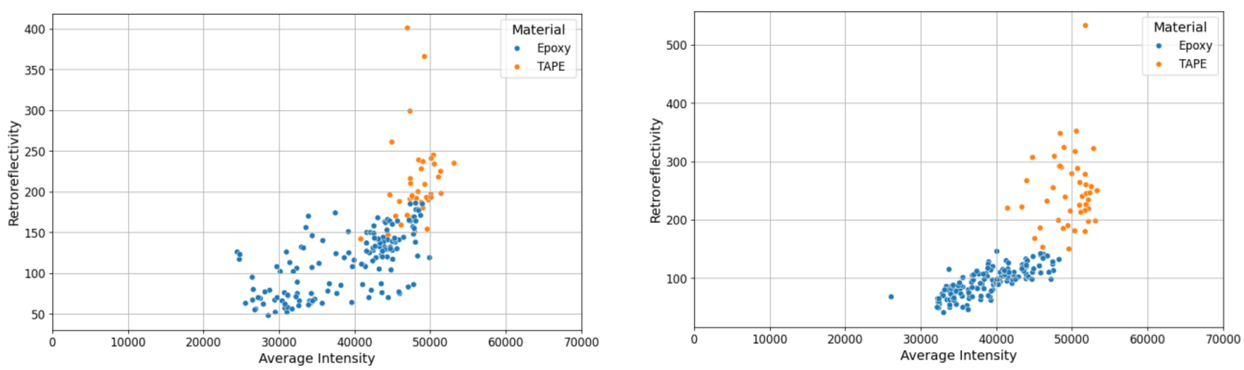

Figure 5-2 I-84 Right Edge Line: a) Eastbound and b) Westbound

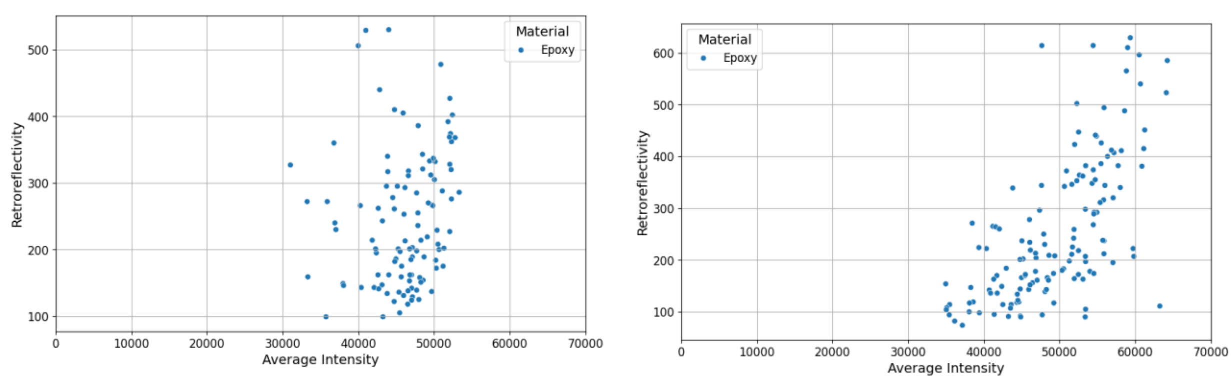

Figure 5-3 I-80 Right Edge Line: a) Eastbound and b) Westbound

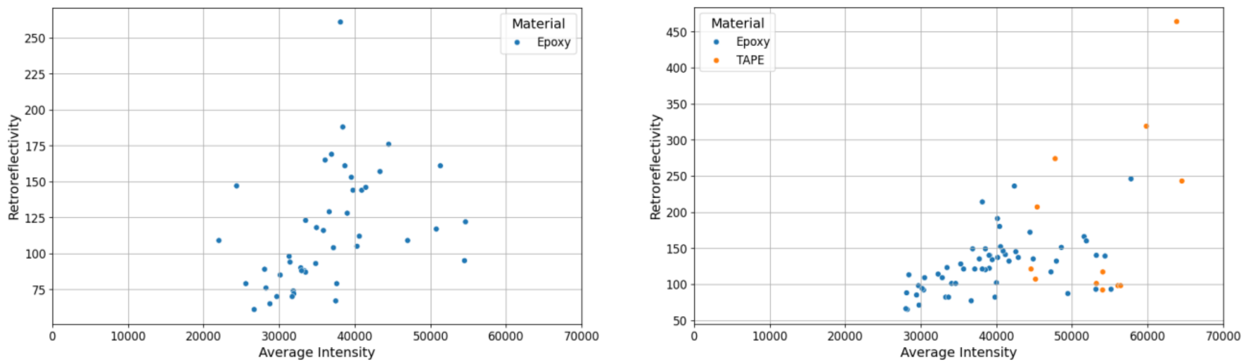

Figure 5-4 I-215 Right Edge Line: a) Northbound and b) Southbound

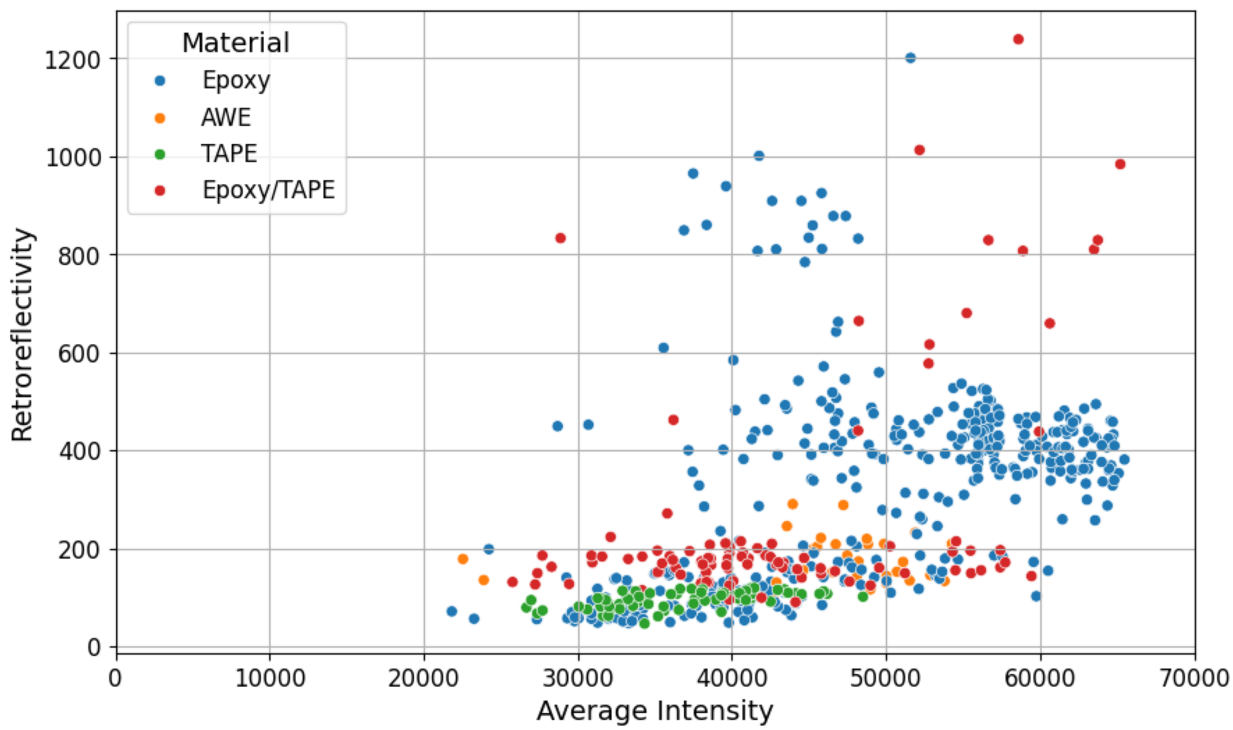

Figure 5-5 I-15 Right Edge Line Both Directions

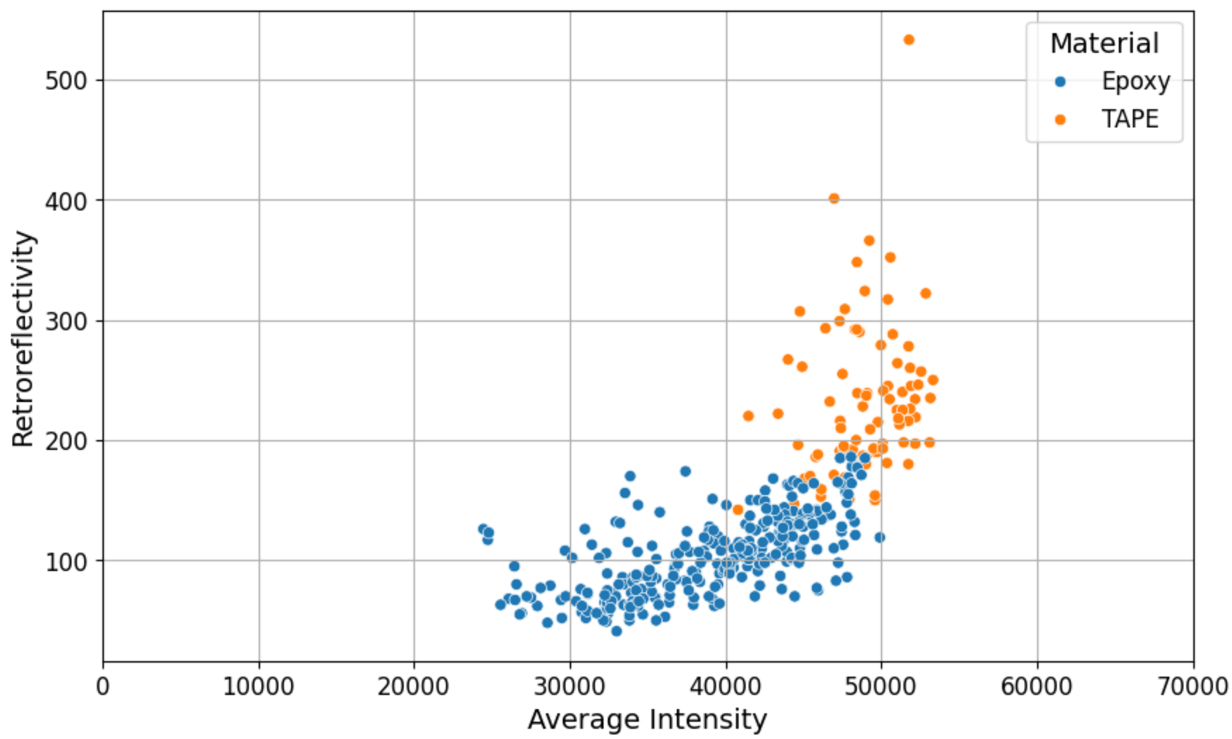

Figure 5-6 I-84 Right Edge Line Both Directions

5.1.2 Left Edge Line

Figures 5-7 to 5-12 illustrate scatter plots comparing field-measured retroreflectivity with average LiDAR intensity values for the left-edge-line scenarios. These figures follow the same format used for the right edge line above; thus, the last two figures include the data for the combined two directions of travel for I-15 and I-84.

It is noted that for freeway sections with a varying number of lanes, separate models may need to be developed to account for the different incidence angle in the LiDAR intensity, as shown in the next section.

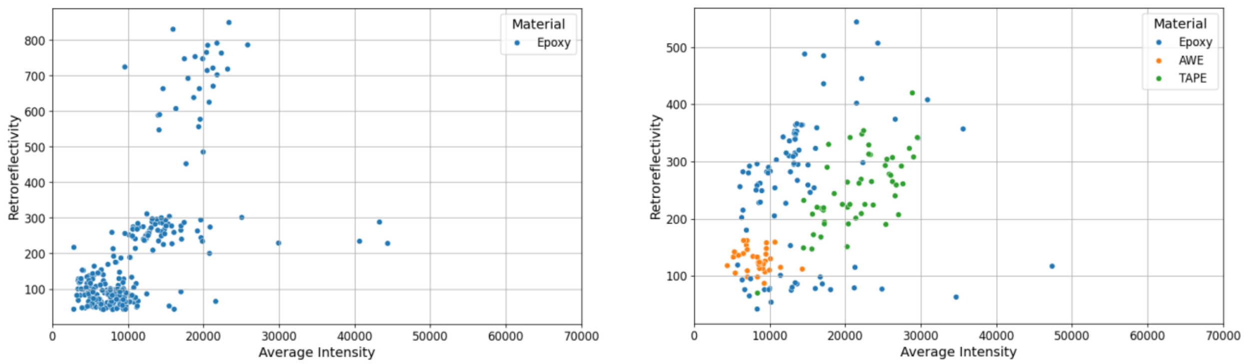

Figure 5-7 I-15 Left Edge Line: a) Northbound and b) Southbound

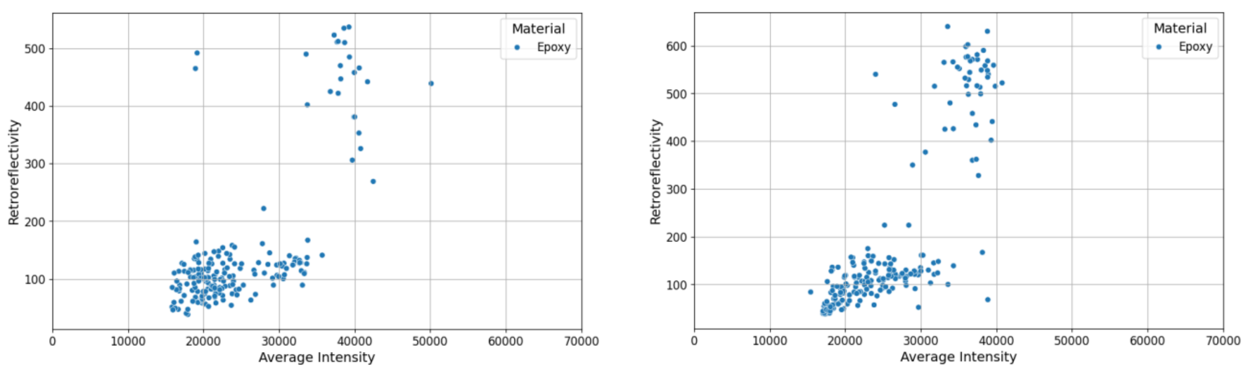

Figure 5-8 I-84 Left Edge Line: a) Eastbound and b) Westbound

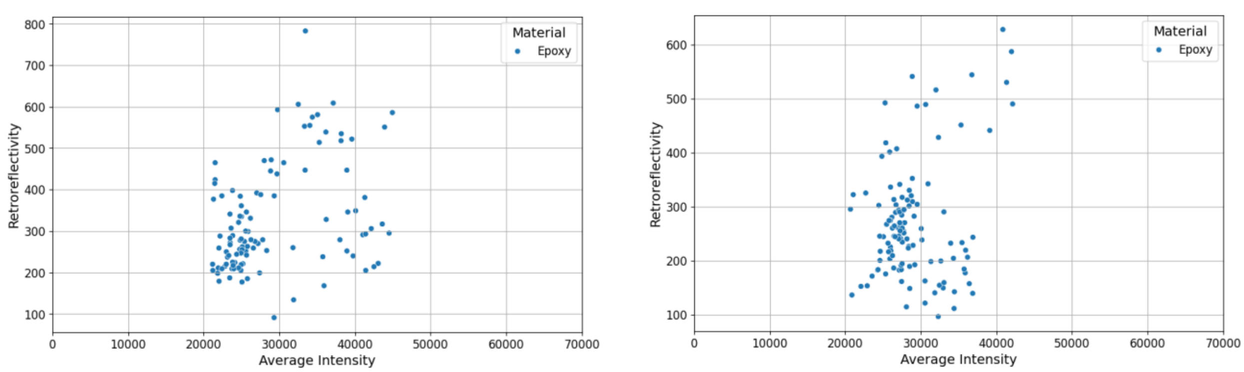

Figure 5-9 I-80 Left Edge Line: a) Eastbound and b) Westbound

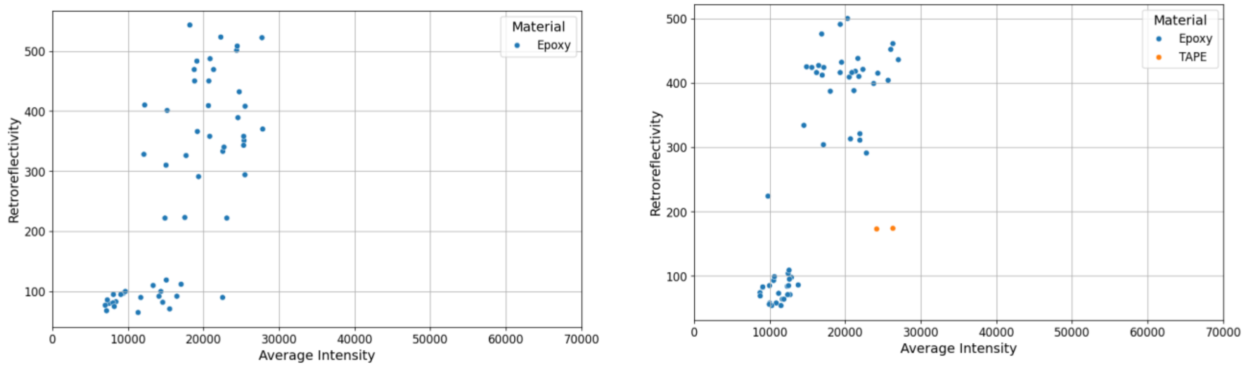

Figure 5-10 I-215 Left Edge Line: a) Northbound and b) Southbound

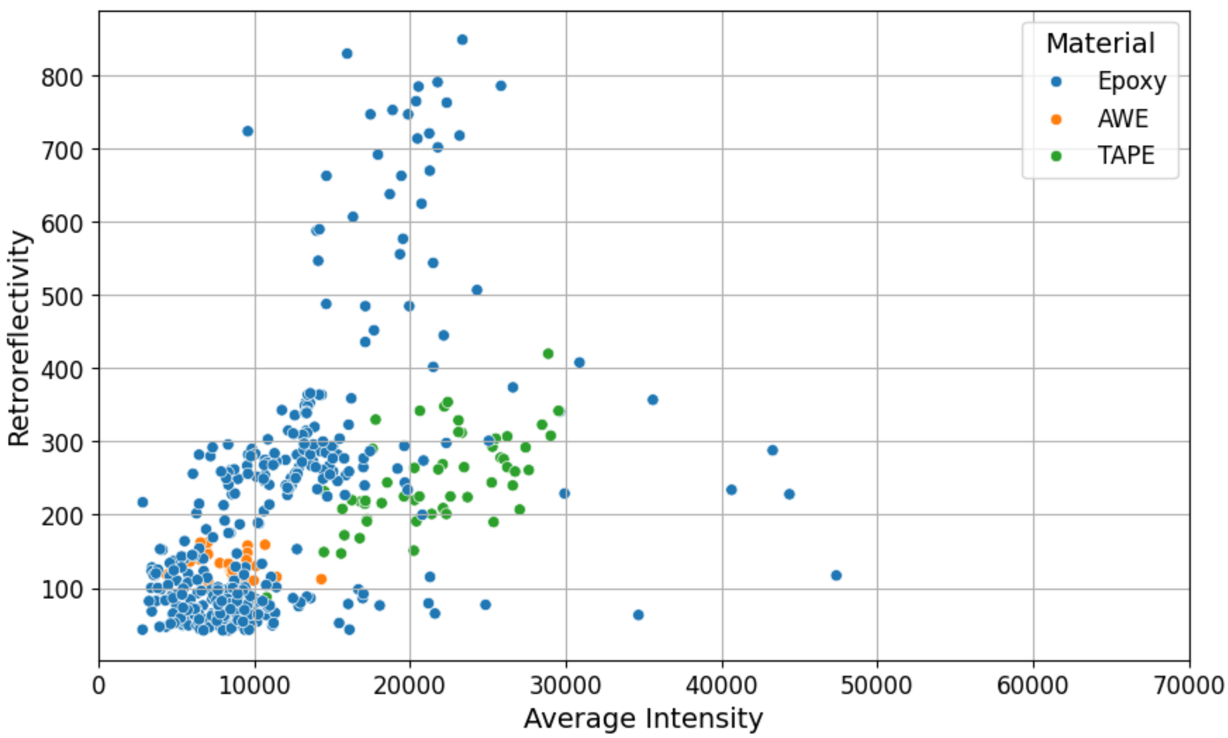

Figure 5-11 I-15 Left Edge Line Both Directions

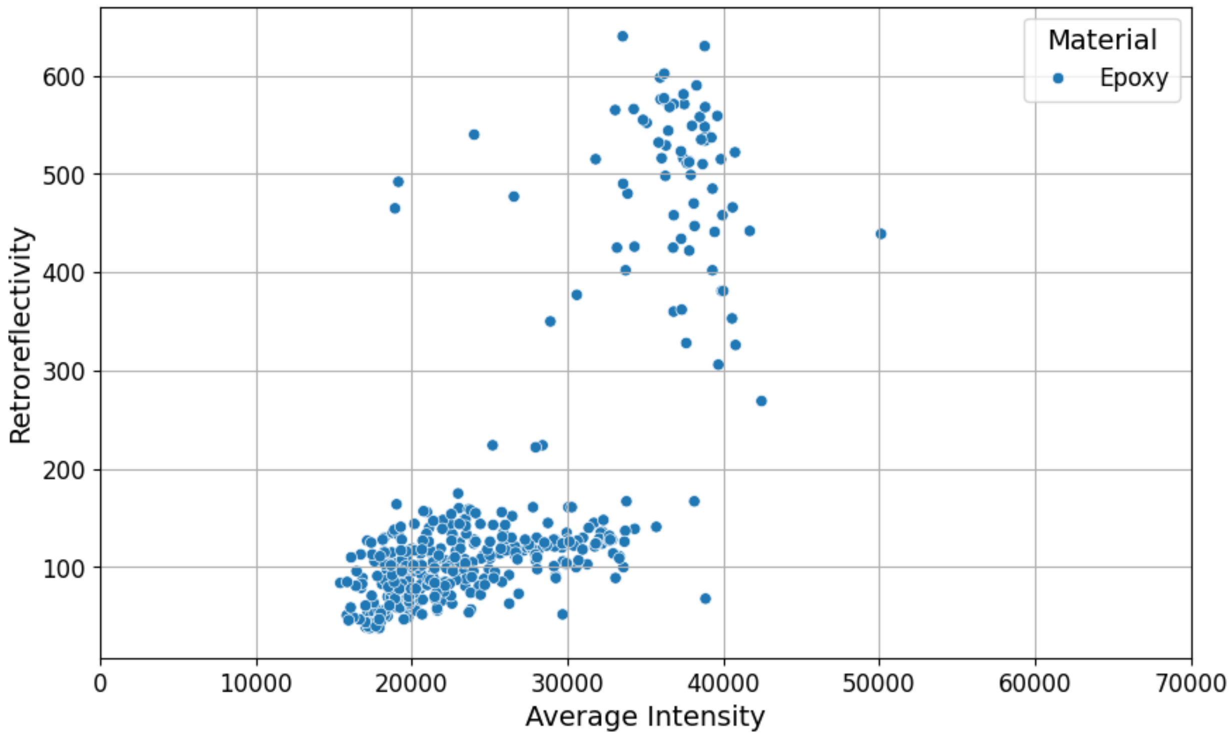

Figure 5-12 I-84 Left Edge Line Both Directions

5.1.3 Dashed Lines

Lastly, Figures 5-13 to 5-15 illustrate scatter plots comparing field-measured retroreflectivity with average LiDAR intensity for the dashed lines. The data collection reflects dashed line data for I-84 and I-80 as illustration examples. On I-84, only 2-lane sections were found in the analysis boundaries, resulting in a single dashed line, whereas I-80 datasets contained segments with 3 lanes and 4 lanes, resulting in two separate modeling efforts.

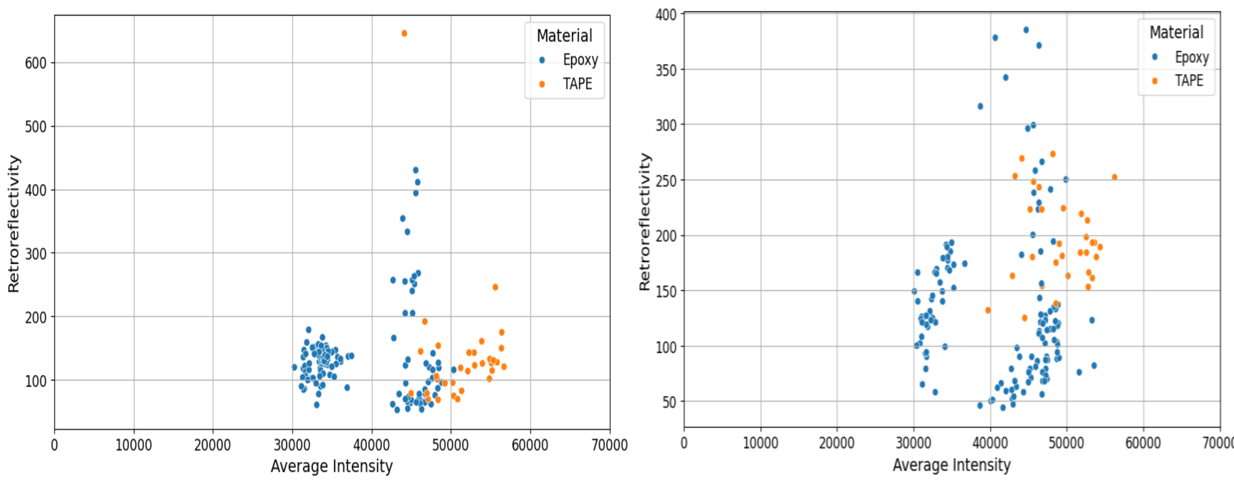

Figure 5-13 I-84 Dashed Line: a) Eastbound and b) Westbound

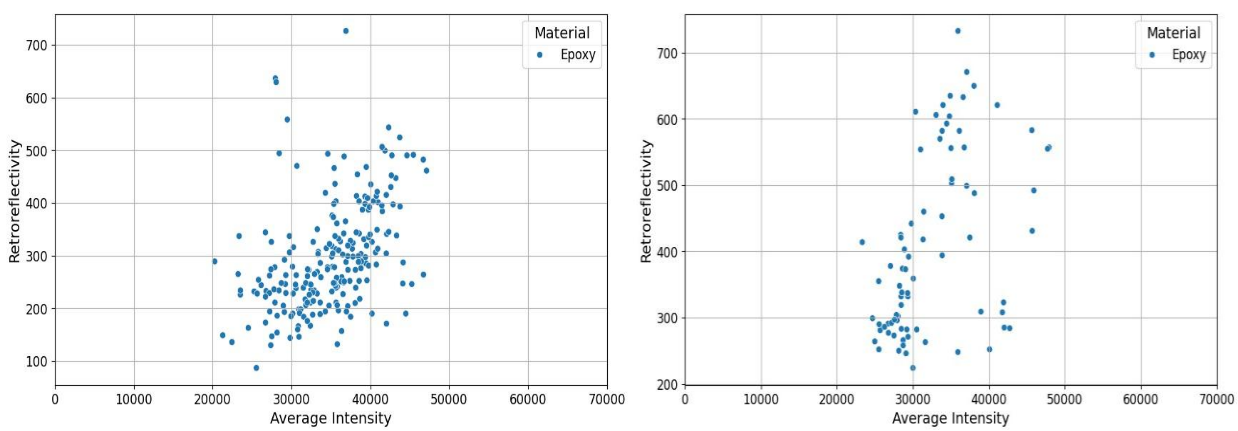

Figure 5-14 I-80 Dashed Line 1: a) 3-Lane Sections and b) 4-Lane Sections

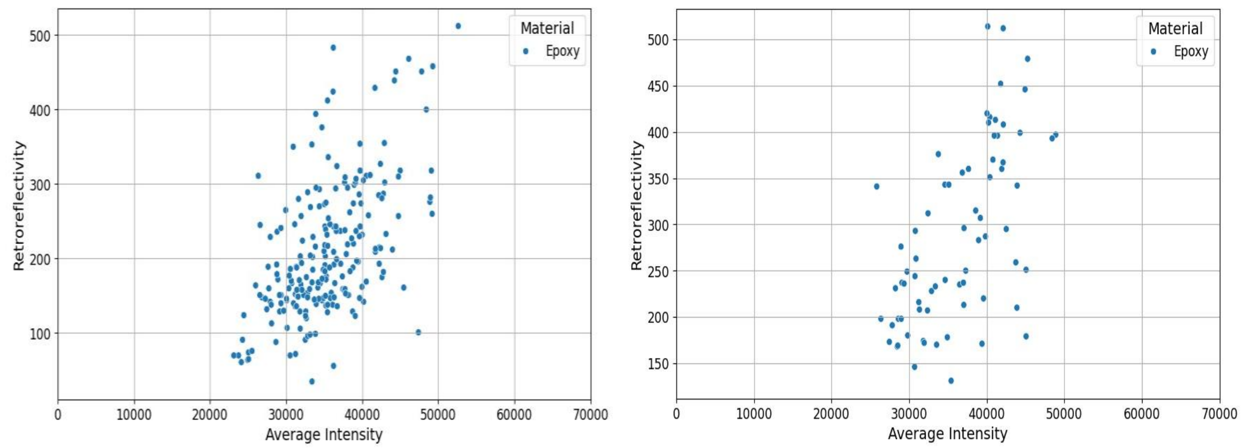

Figure 5-15 I-80 Dashed Line 2: a) 3-Lane Sections and b) 4-Lane Sections

5.2 Regression Models

Key performance metrics from selected models using an exponential regression and the XGBoost model, including the RMSE and R^2, are summarized in Tables 5-1 through 5-3 for the right edge line, the left edge line, and the dashed lines, correspondingly.

Overall, the performance of XGBoost displays superior correlation to outcomes from the exponential regression, as expected from the flexibility that the machine learning technique offers. This is generally true as long as the data is sufficient for both training and testing steps.

In terms of RMSE, both the exponential regression and XGBoost exhibit errors that range between about 20-110 mcd/m^2/lux. To put these errors into context, a reading of about 400 mcd/m^2/lux of retroreflectivity would be expected to vary by such amounts above or below, on average. In reality, greater values would tend to have greater absolute deviations, as is observed below in the modeling results, so typical errors for high retroreflectivity areas could be closer to 110, but lower levels would be closer to 20. This also indicates that errors for lower readings closer to a low threshold (e.g., 100 mcd/m^2/lux) will tend to be smaller, which in turn will lead to more comfortable uncertainty ranges for individual readings at key retroreflectivity levels.

Table 5-1 Performance Metrics Summary for the Right Edge Line

Road Marking	RMSE		R^2	
	Exponential	XGBoost	Exponential	XGBoost
I-15 REL NB	76	73	0.64	0.68
I-15 REL SB	83	74	0.74	0.79
I-15 REL Both Directions	87	70	0.63	0.76
I-84 REL EB	21	20	0.78	0.8
I-84 REL WB	27	23	0.79	0.86
I-84 REL Both Directions	29	25	0.68	0.78

Table 5-2 Performance Metrics Summary for the Left Edge Line

Road Marking	RMSE		R^2	
	Exponential	XGBoost	Exponential	XGBoost
I-15 LEL NB	110	96	0.67	0.75
I-15 LEL SB	78	61	0.31	0.58
I-84 LEL EB	58	47	0.74	0.8
I-84 LEL WB	68	46	0.86	0.94
I-84 LEL Both Directions	92	58	0.65	0.86

Table 5-3 Performance Metrics Summary for the Dashed Lines

Road Marking	RMSE		R^2	
	Exponential	XGBoost	Exponential	XGBoost
I-15 REL NB	67	61	0.71	0.76
I-15 REL SB	85	74	0.75	0.81
I-15 REL Both Directions	99	88	0.55	0.66
I-84 REL EB	25	25	0.74	0.74
I-84 REL WB	28	25	0.81	0.85
I-84 REL Both Directions	25	24	0.79	0.80

The modeling results for an extended set of lane marking groups are included in Figures 5-16 through 5-32. Each figure illustrates outcomes obtained with the exponential models and XGBoost using datasets without outliers and normalized between 0 and 1. Subfigures labeled as "a)" show the exponential model results, whereas subfigures "b)" show the outcomes from XGBoost. In addition, the XGBoost shows training data points on the top plot within the "b)" subfigures, exhibiting about 80% of the average cross-validation sample, compared to the average 20% of the sample used for testing purposes and shown on the lower plot.

The data is organized as follows:

- Right edge line:
    - I-15 northbound, southbound, and both directions (Figures 5-16 – 5-18)
    - I-84 eastbound, westbound, and both directions (Figures 5-19 – 5-21)
- Left edge line (models by number of lanes):
    - I-15 both directions – 3-lane, 4-lane, and 5-lane sections (Figures 5-22 – 5-24)
    - I-80 both directions – 3-lane sections (Figure 5-25)
    - I-84 eastbound, westbound, and both directions – 2-lane sections (Figures 5-26 – 5-28)
- Dashed lines 1 and 2:
    - Dashed lines 1: I-80 both directions – 3-lane, 4-lane sections (Figures 5-29, 5-30)
    - Dashed lines 2: I-80 both directions – 3-lane, 4-lane sections (Figures 5-31, 5-32)

It is important to mention that the figure breakdown is intended to illustrate the models across different lane marking types and roadway section configurations (when applicable). For example, models for the right edge lines do not need to be divided into different roadway section configurations since the data collection van typically travels on the right lane, avoiding different angles of incidence in the data for different cross sections (2, 3, or 4 lanes). However, the left edge line and the dashed lines may have variations due to occlusion and the LiDAR angle, as the distance from the van to the target lane changes with the number of lanes in the cross section.

Overall, all models exhibit a clear non-decreasing trend as the x-axis range moves from 0 to 1, even in cases where data is not available throughout the full range or when it is concentrated in clusters. A good example of a densely populated range is Figure 5-21 for both directions along the right edge line of I-84, where both the regression and the XGBoost algorithms depict what could be regarded as typical expected trends. On the other hand, an example of sparse data can be observed in Figure 5-26, for the eastbound left edge line also on I-84, where most data exhibits low retroreflectivity values near 100 mcd/m^2/lux with few data points in the 400-500 range. Here it is also clear how the XGBoost model provides an advantage over the regression, as the regression is only capable of producing a single trendline, but XGBoost can adapt to more sudden changes in the trend, particularly for points above 0.6 on the x-axis, where the predictions closely follow the actual data points after the increase in retroreflectivity both in the training and testing plots.

In general, models for different cross sections along a given freeway exhibited an expected trend, with models for narrower cross sections showing lower variations (e.g., Figure 5-22, I-15 left-edge line points from 3-lane sections) compared to segments with wider cross-sections (e.g., Figure 5-24, I-15 left-edge line points from 5-lane sections).

This is also true for the dashed lines, which provided expected general non-decreasing and model-conforming trends, with smaller LiDAR intensity variations for the dashed line 2 (closer to the right edge lane and the data collection van) compared to the dashed line 1. The dashed lines also showed lower variations for narrower sections compared to those from wider sections (e.g., lower variations for 3-lane sections compared to 4-lane sections). However, even for wider sections, models for the dashed lines could be considered suitable for accurate predictions, particularly along lower retroreflectivity values.

A final takeaway from the regression models is that despite their ability to generate overall consistent trends, these methods fail to take advantage of improved outcomes that could be obtained if spatial correlations between points are taken into account. Classification models provide a suitable solution to incorporate this feature, as described in the following section.

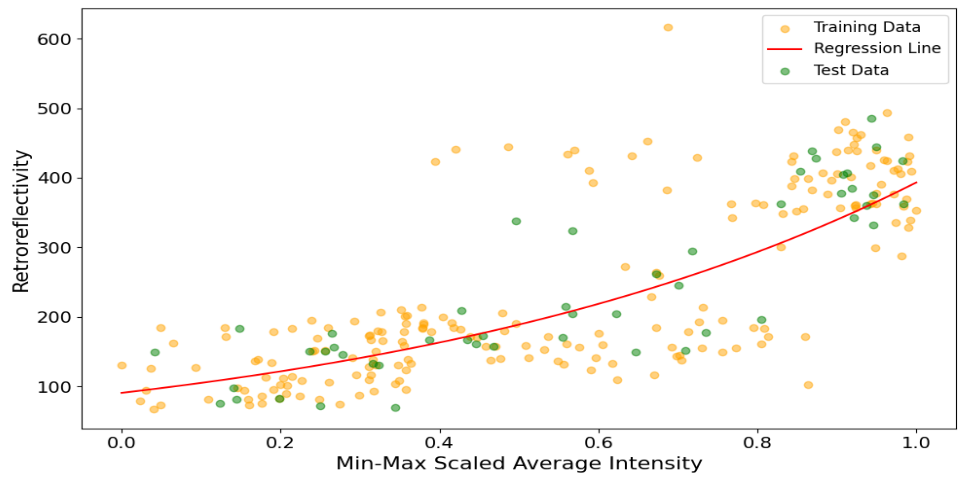

a) I-15 Right Edge Line - Northbound – Normalized Data and Exponential Model

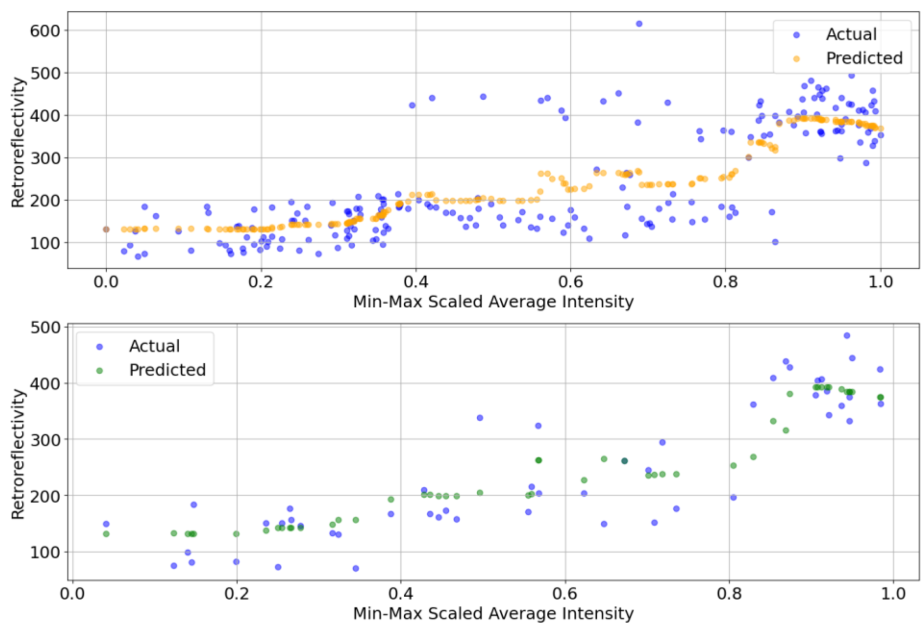

b) I-15 Right Edge Line - Northbound – Normalized Data and XGBoost Model

Figure 5-16 I-15 Right Edge Line - Northbound

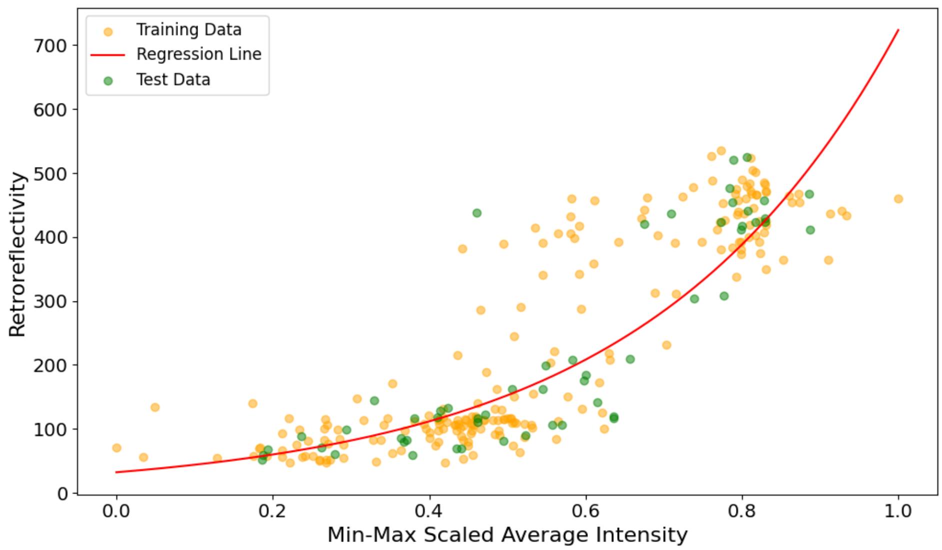

a) I-15 Right Edge Line - Southbound – Normalized Data and Exponential Model

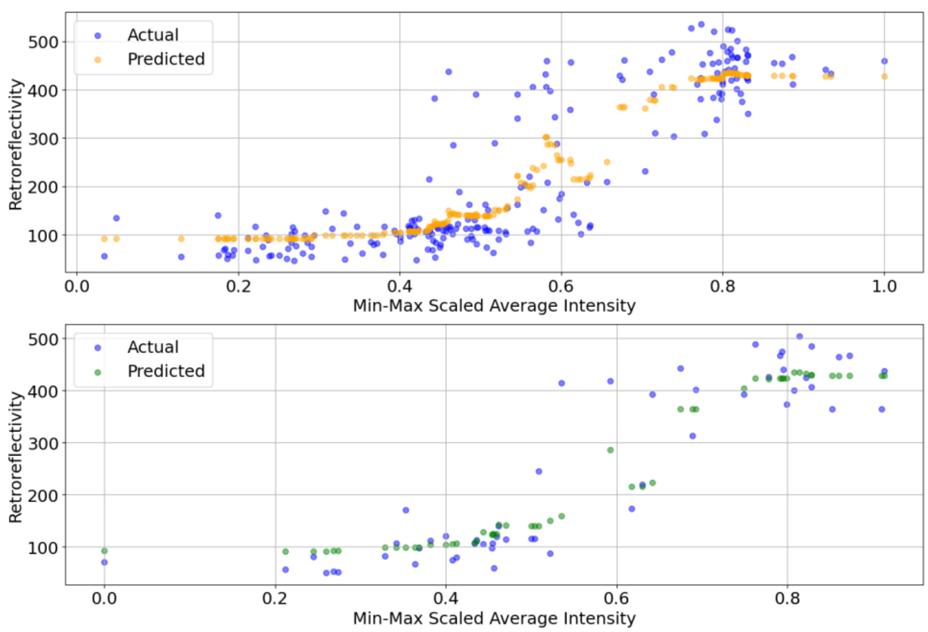

b) I-15 Right Edge Line - Southbound – Normalized Data and XGBoost Model

Figure 5-17 I-15 Right Edge Line - Southbound

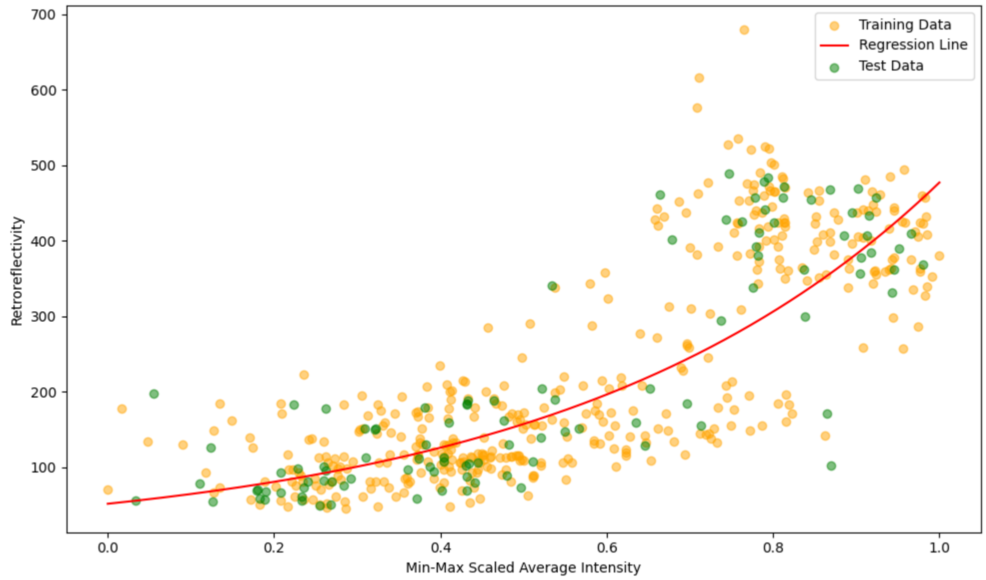

a) I-15 Right Edge Line – Both Directions – Normalized Data and Exponential Model

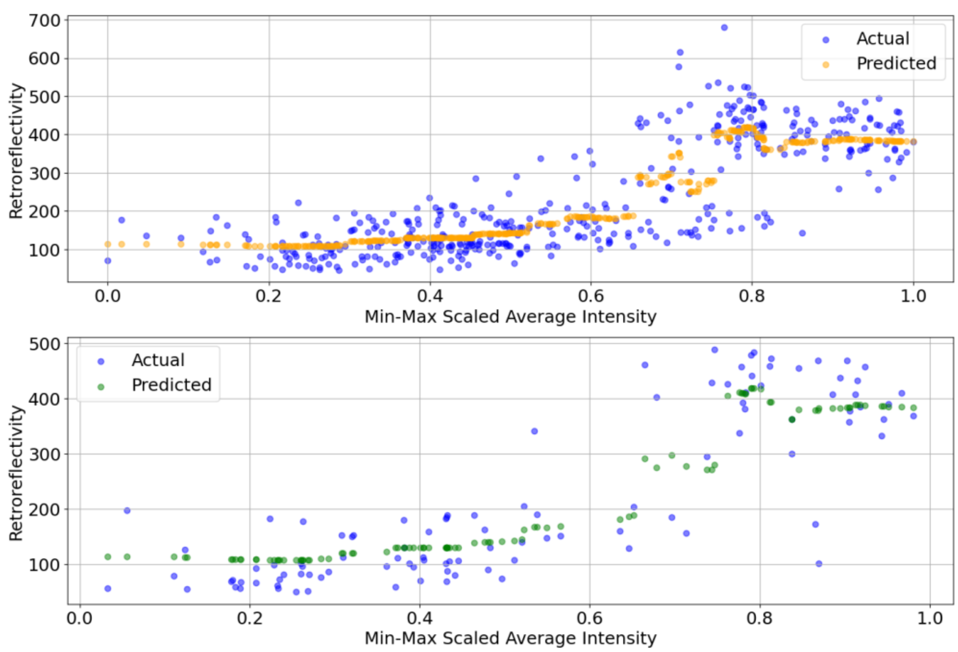

b) I-15 Right Edge Line – Both Directions – Normalized Data and XGBoost Model

Figure 5-18 I-15 Right Edge Line - Both Directions

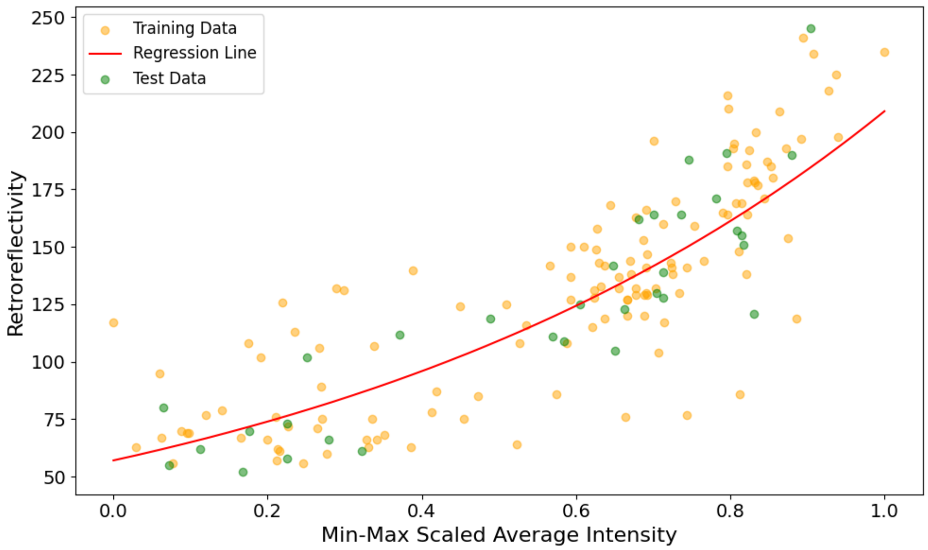

a) I-84 Right Edge Line – Eastbound – Normalized Data and Exponential Model

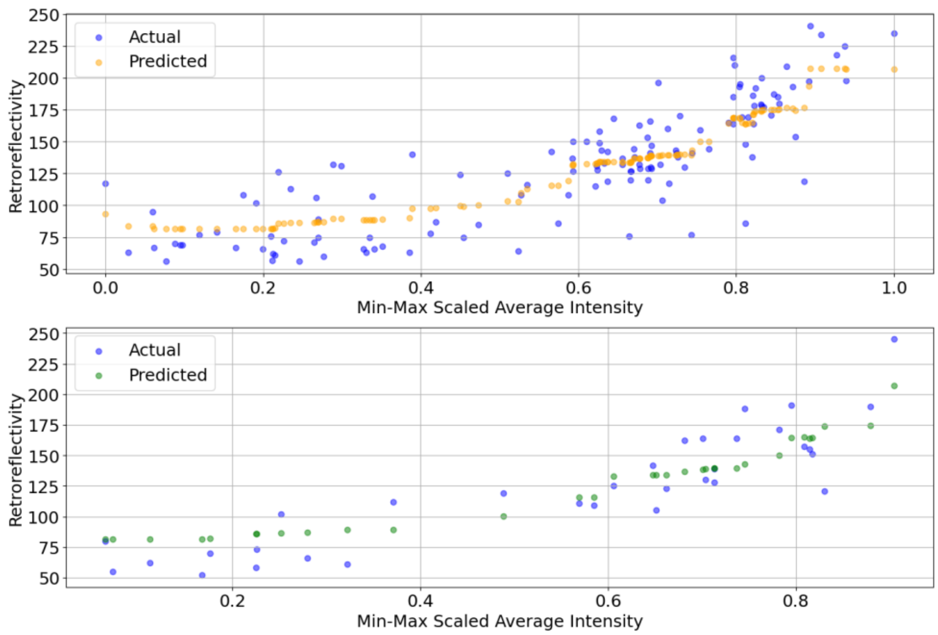

b) I-84 Right Edge Line – Eastbound – Normalized Data and XGBoost Model

Figure 5-19 I-84 Right Edge Line – Eastbound

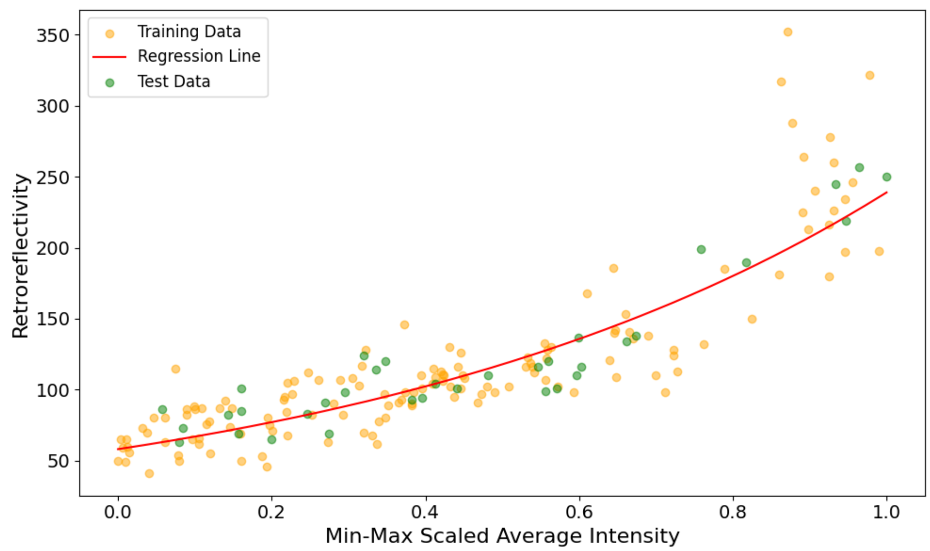

a) I-84 Right Edge Line – Westbound – Normalized Data and Exponential Model

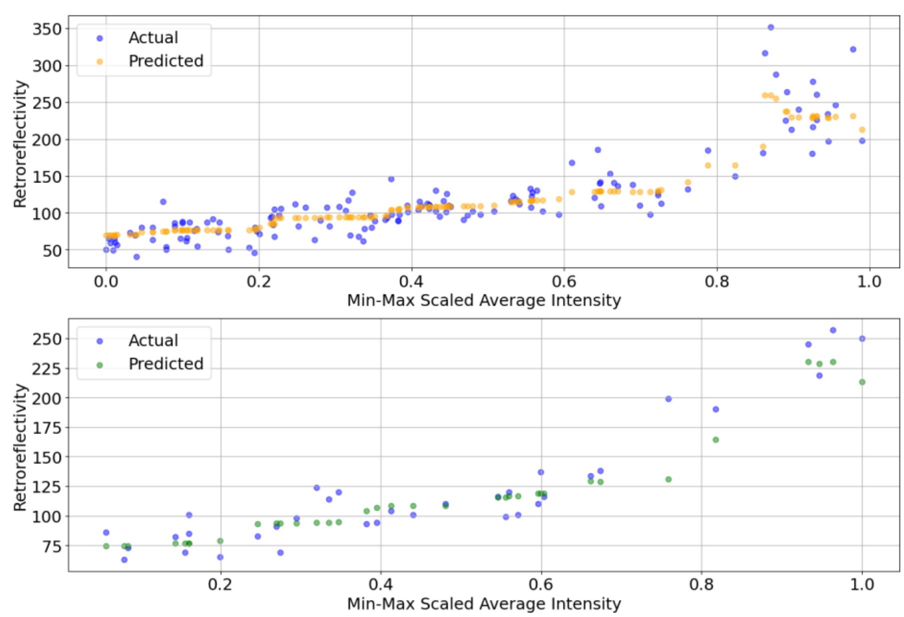

b) I-84 Right Edge Line – Westbound – Normalized Data and XGBoost Model

Figure 5-20 I-84 Right Edge Line – Westbound

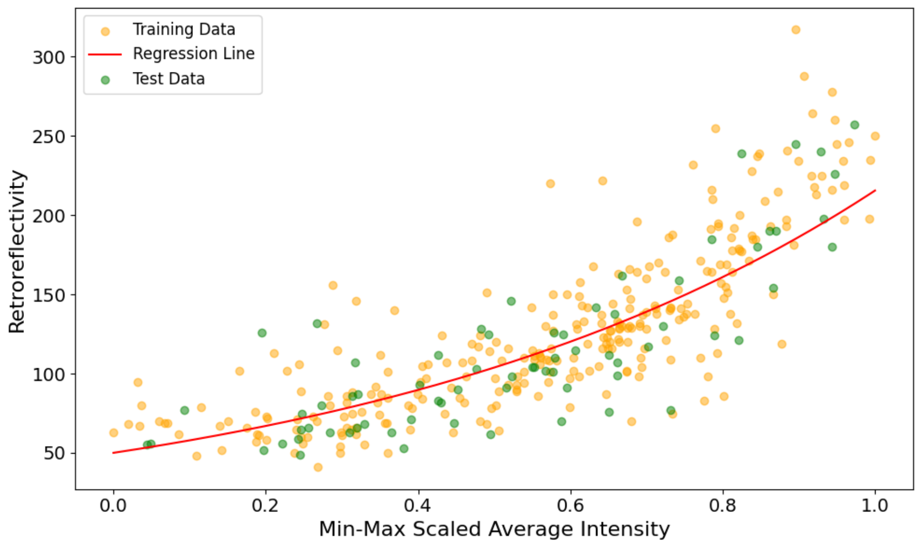

a) I-84 Right Edge Line – Both Directions – Normalized Data and Exponential Model

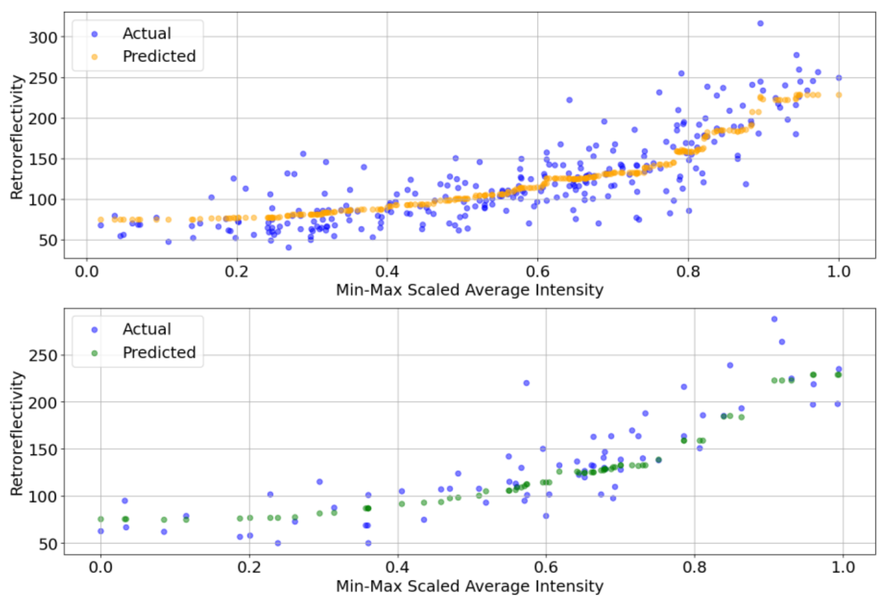

b) I-84 Right Edge Line – Both Directions – Normalized Data and XGBoost Model

Figure 5-21 I-84 Right Edge Line – Both Directions

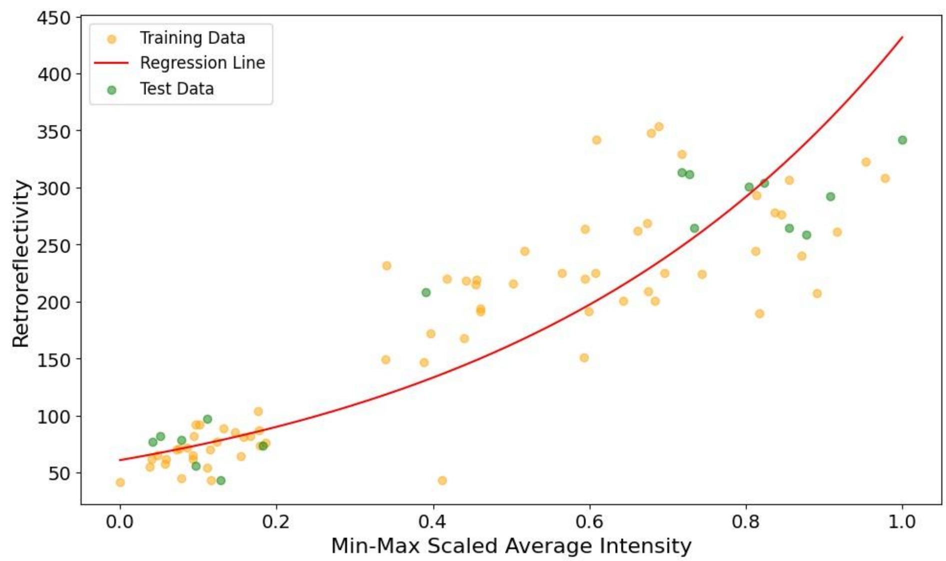

a) I-15 Left Edge Line – 3-Lane Sections – Normalized Data and Exponential Model

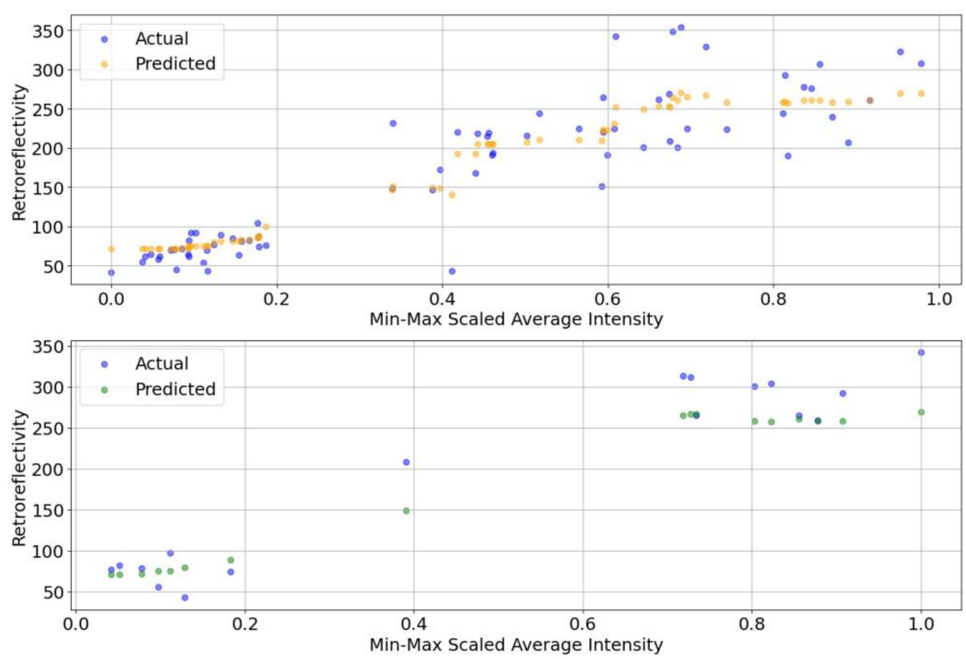

b) I-15 Left Edge Line – 3-lane Sections – Normalized Data and XGBoost Model

Figure 5-22 I-15 Left Edge Line – 3-Lane Sections

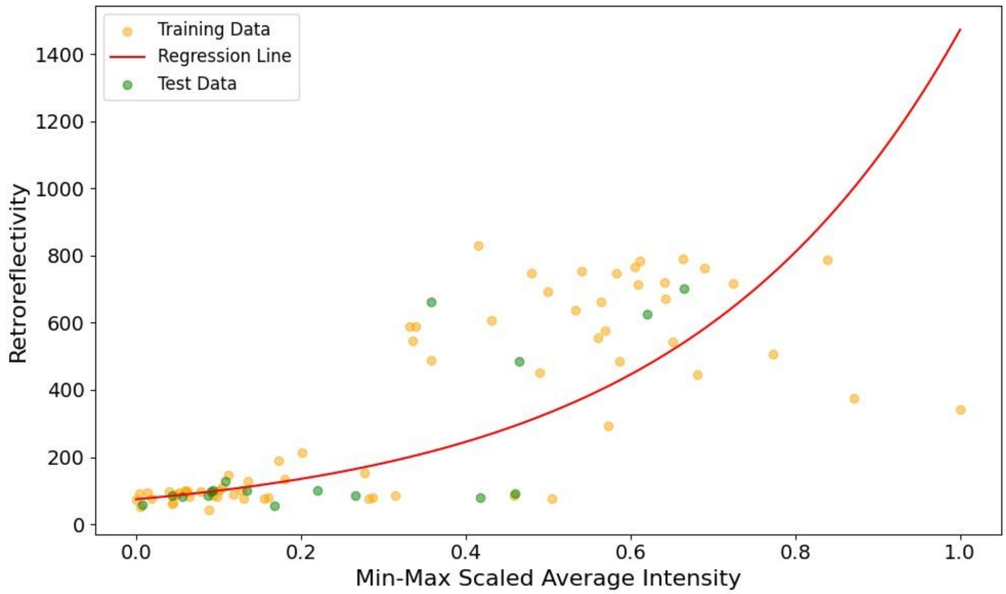

a) I-15 Left Edge Line – 4-Lane Sections – Normalized Data and Exponential Model

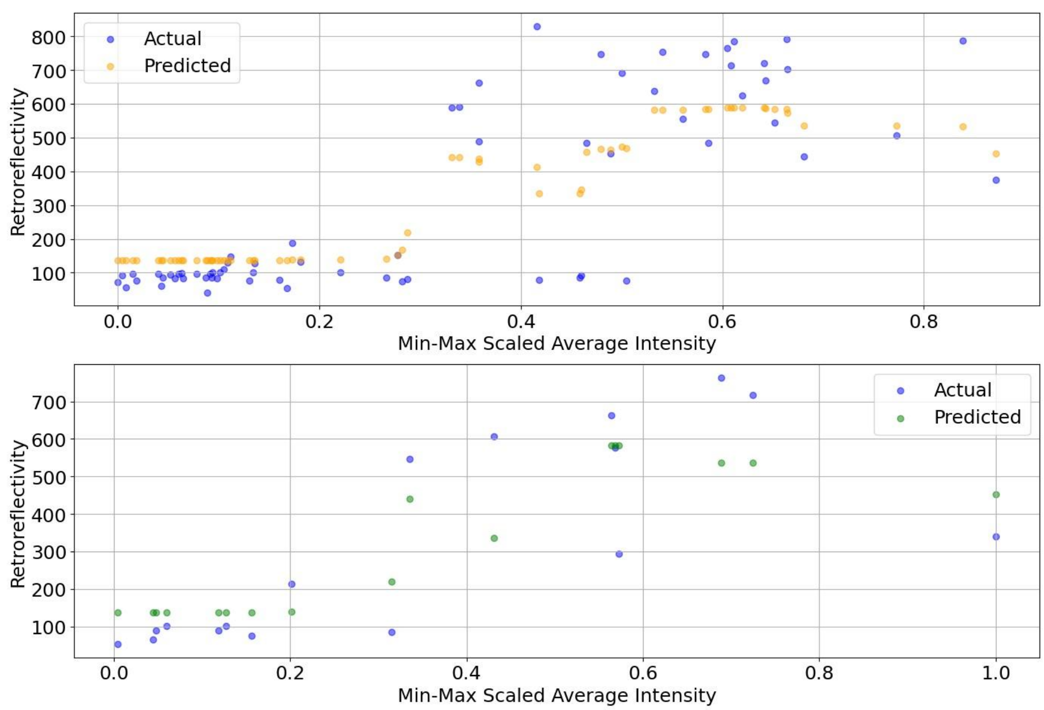

b) I-15 Left Edge Line – 4-Lane Sections – Normalized Data and XGBoost Model

Figure 5-23 I-15 Left Edge Line – 4-Lane Sections

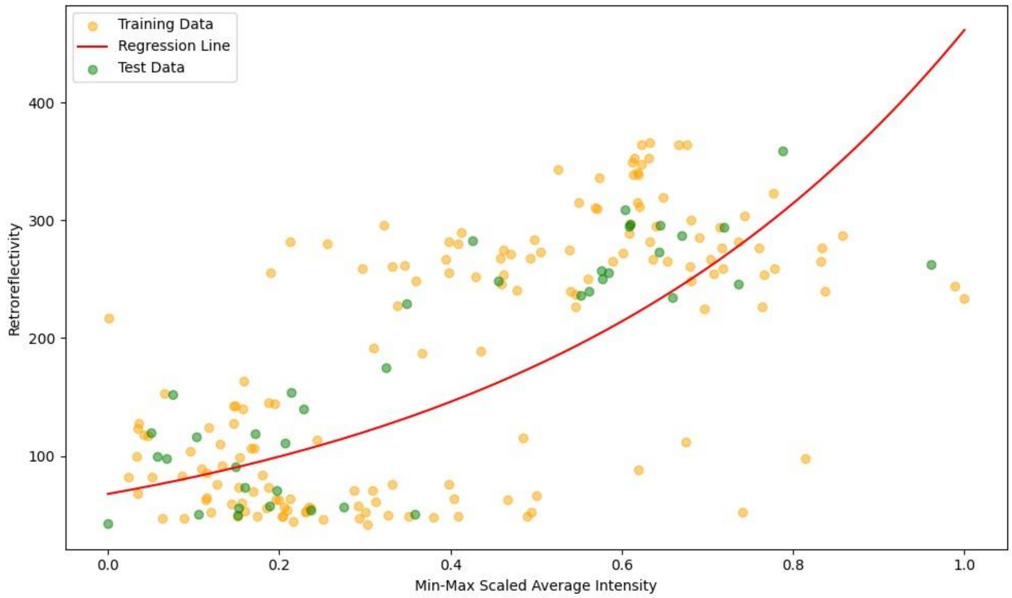

a) I-15 Left Edge Line – 5-Lane Sections – Normalized Data and Exponential Model

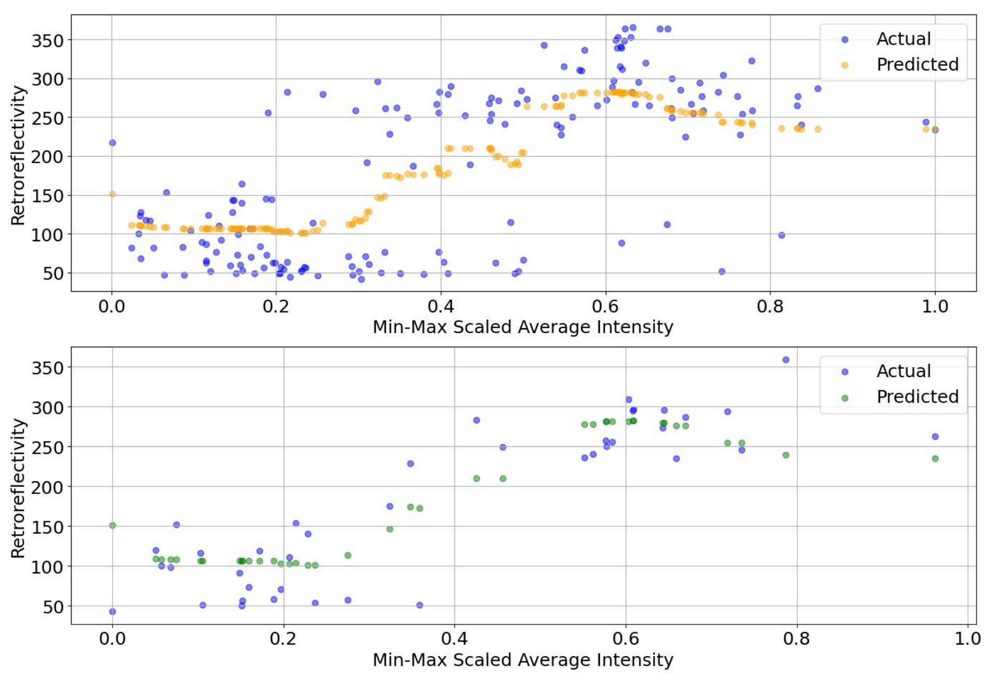

b) I-15 Left Edge Line – 5-Lane Sections – Normalized Data and XGBoost Model

Figure 5-24 I-15 Left Edge Line – 5-Lane Sections

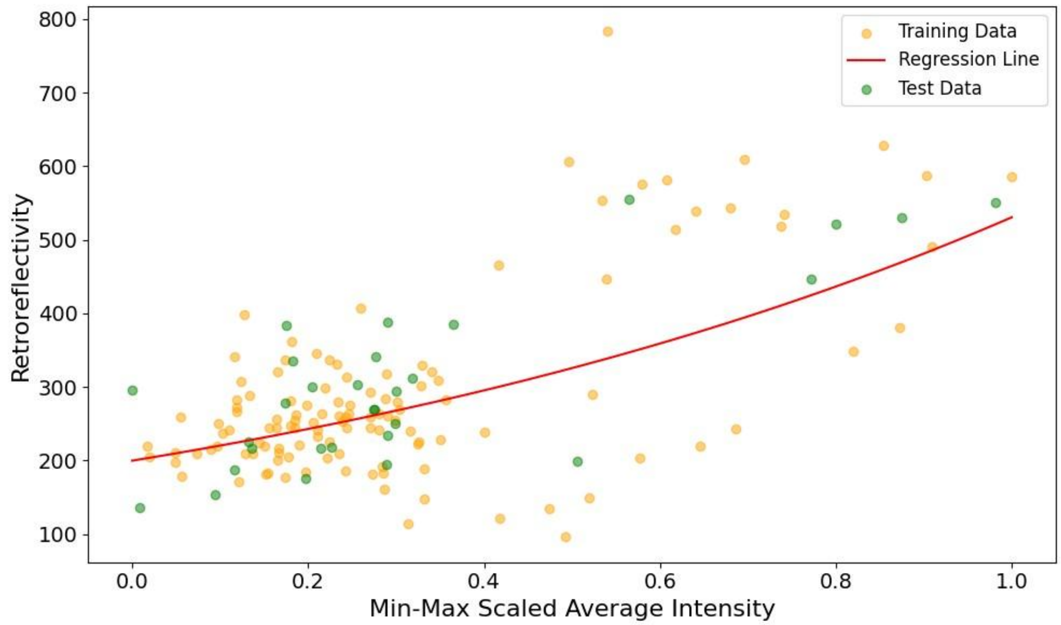

a) I-80 Left Edge Line – 3-Lane Sections – Normalized Data and Exponential Model

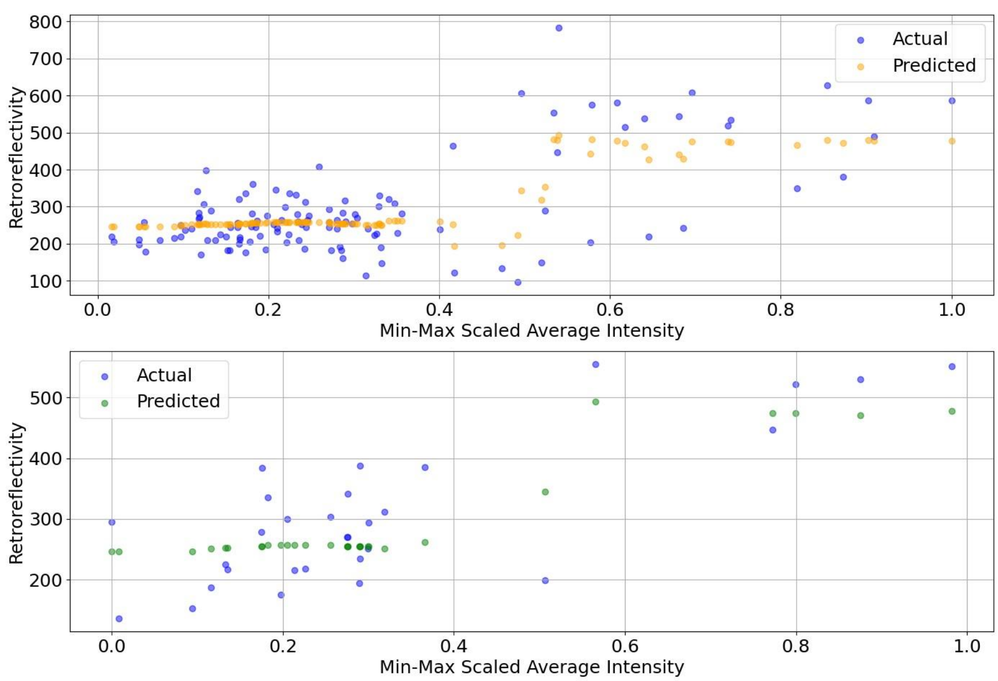

b) I-80 Left Edge Line – 3-Lane Sections – Normalized Data and XGBoost Model

Figure 5-25 I-80 Left Edge Line – 3-Lane Sections

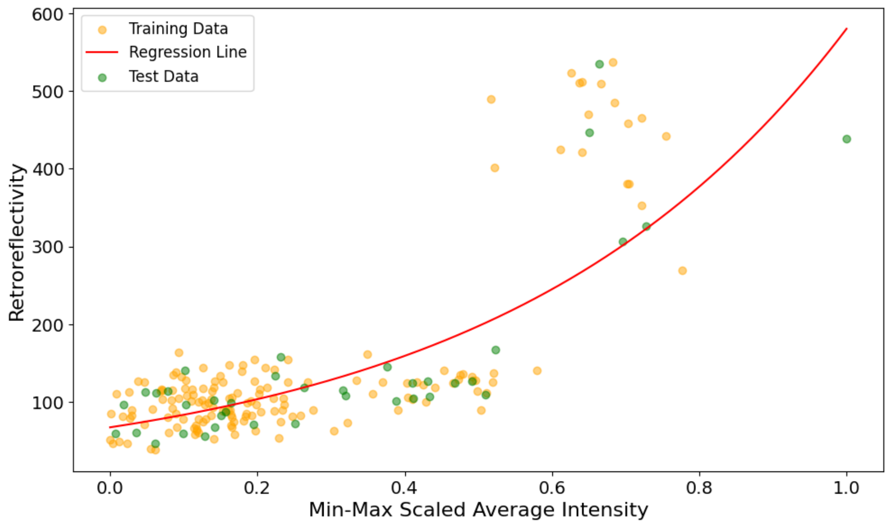

a) I-84 Left Edge Line – Eastbound – Normalized Data and Exponential Model

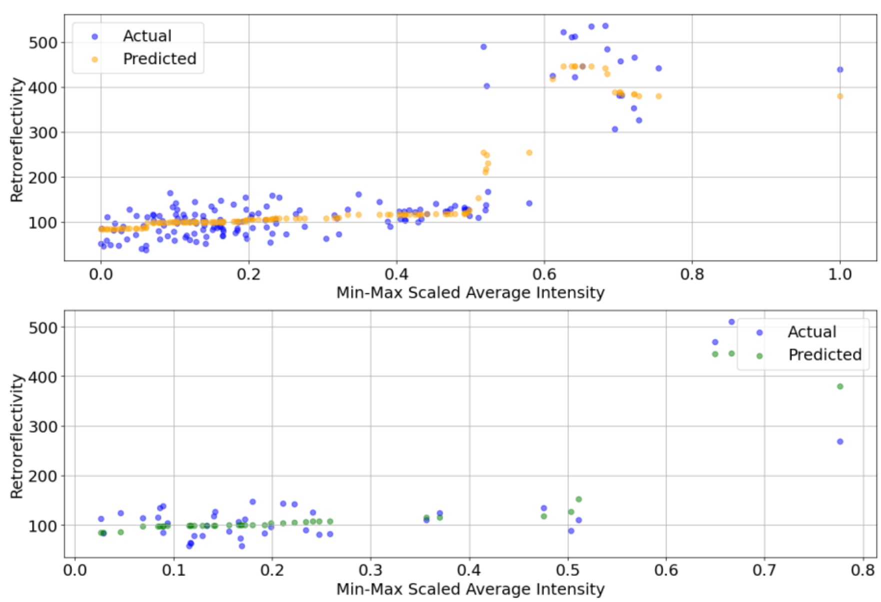

b) I-84 Left Edge Line – Eastbound– Normalized Data and XGBoost Model

Figure 5-26 I-84 Left Edge Line – Eastbound

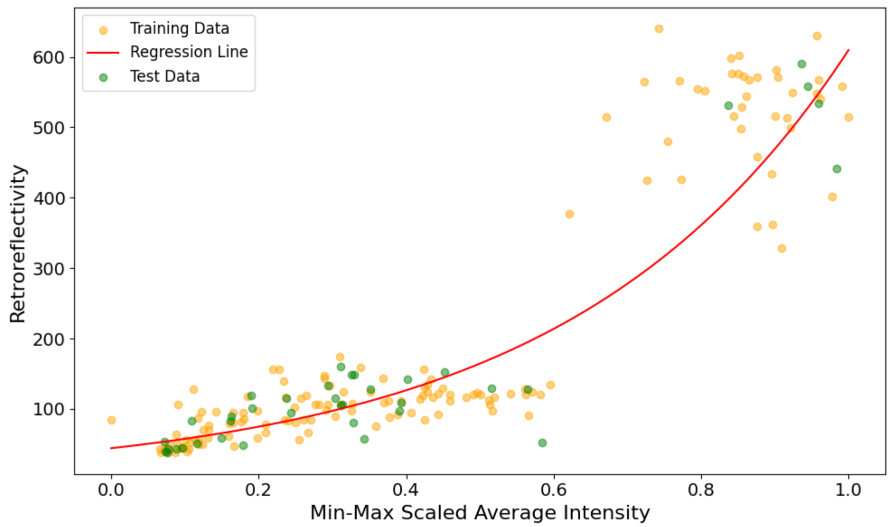

a) I-84 Left Edge Line – Westbound – Normalized Data and Exponential Model

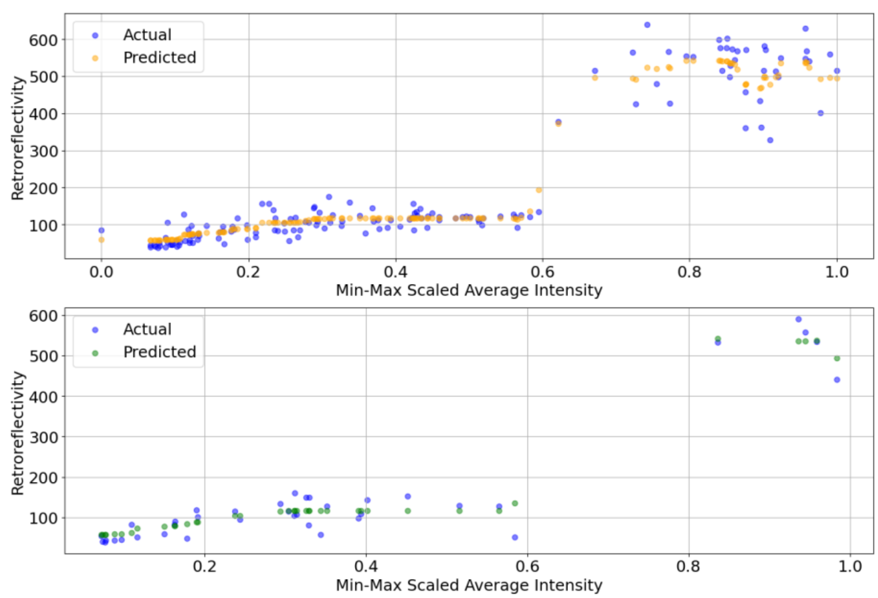

b) I-84 Left Edge Line – Westbound– Normalized Data and XGBoost Model

Figure 5-27 I-84 Left Edge Line – Westbound

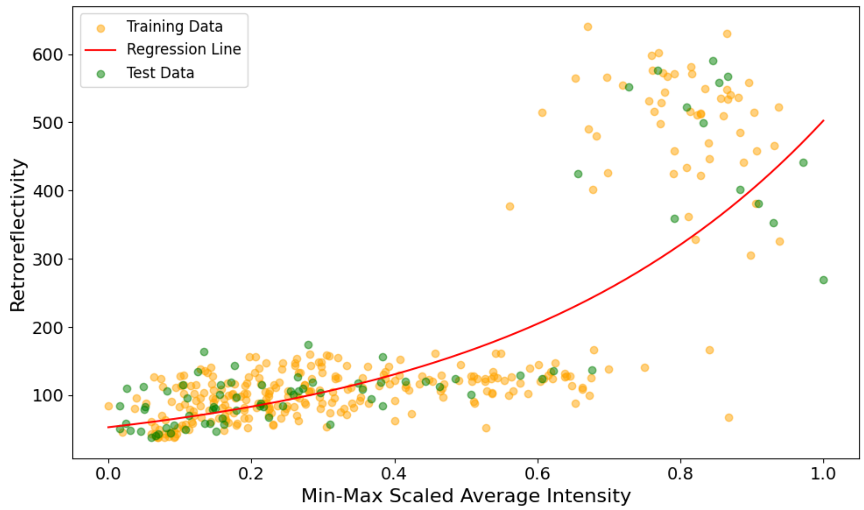

a) I-84 Left Edge Line – Both Directions – Normalized Data and Exponential Model

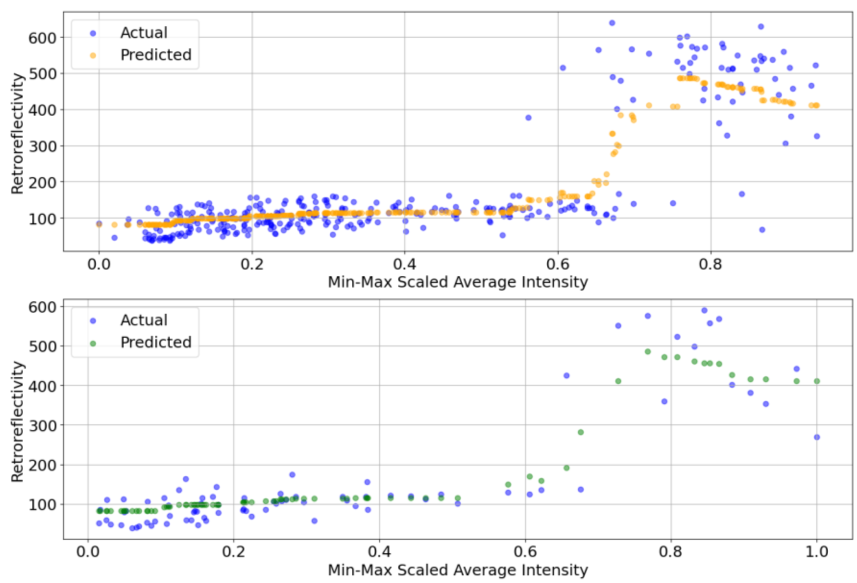

b) I-84 Left Edge Line – Both Directions – Normalized Data and XGBoost Model

Figure 5-28 I-84 Left Edge Line – Both Directions

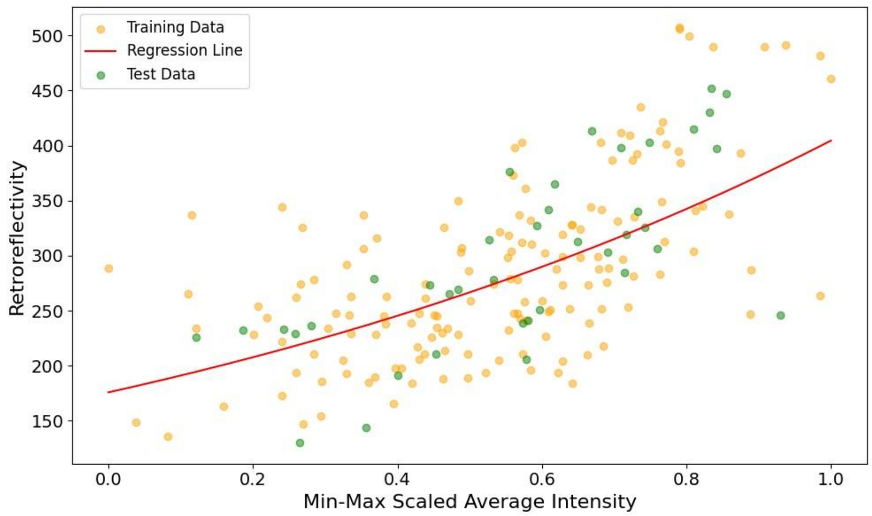

a) I-80 Dashed Line 1 – 3-Lane Sections – Normalized Data and Exponential Model

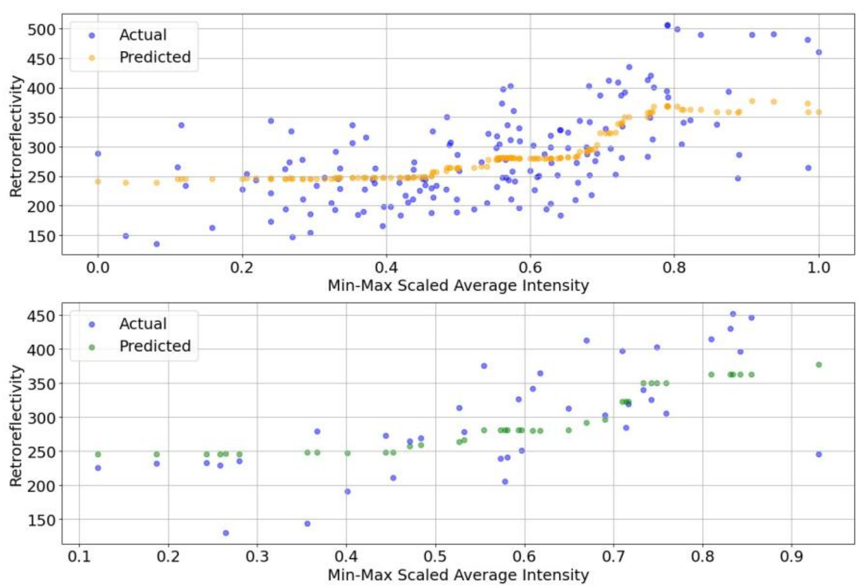

b) I-80 Dashed Line 1 – 3-Lane Sections – Normalized Data and XGBoost Model

Figure 5-29 I-80 Dashed Line 1 – 3-Lane Sections

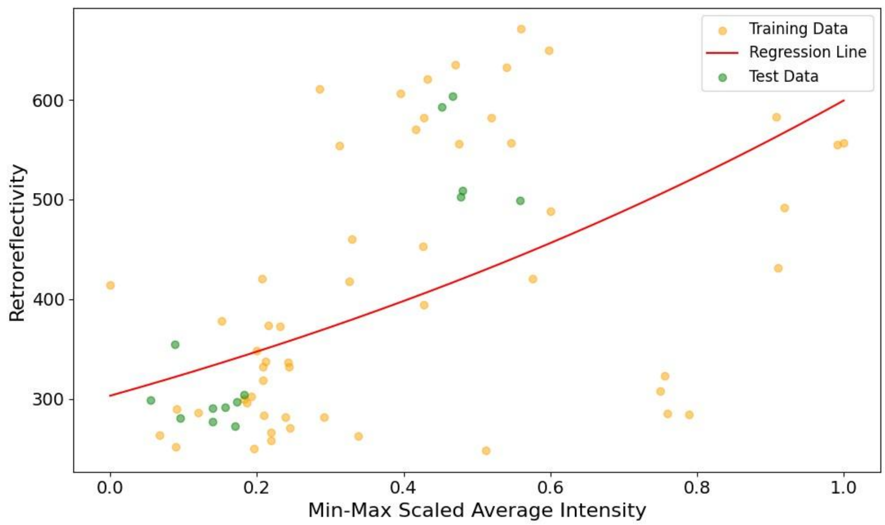

a) I-80 Dashed Line 1 – 4-Lane Sections – Normalized Data and Exponential Model

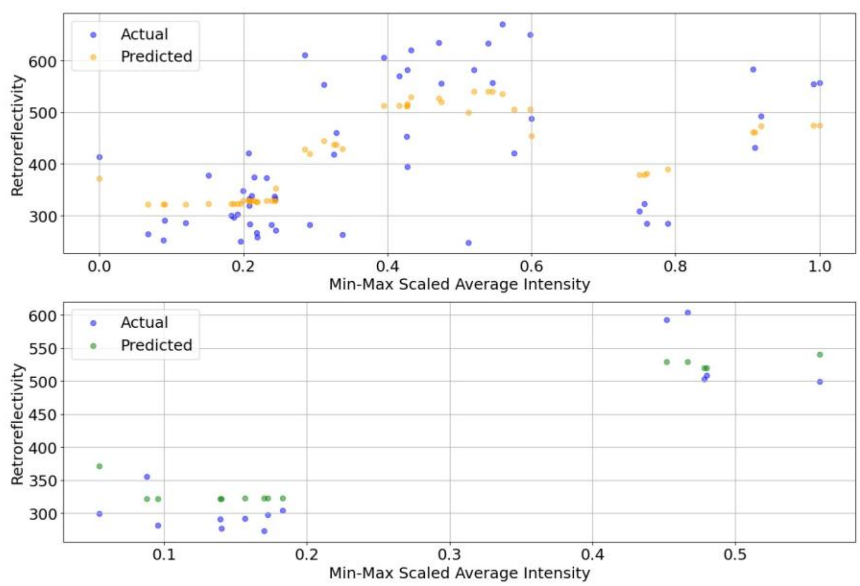

b) I-80 Dashed Line 1 – 4-Lane Sections – Normalized Data and XGBoost Model

Figure 5-30 I-80 Dashed Line 1 – 4-Lane Sections

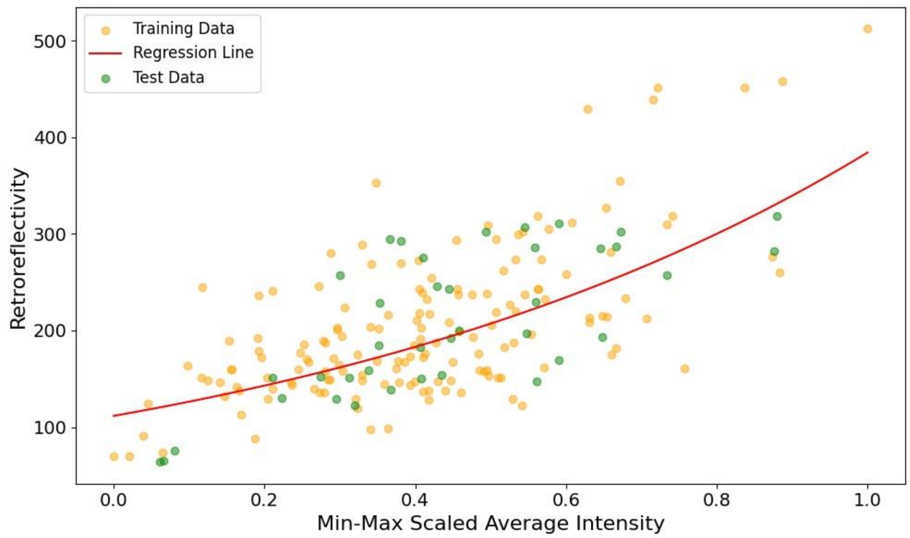

a) I-80 Dashed Line 2 –3-Lane Sections – Normalized Data and Exponential Model

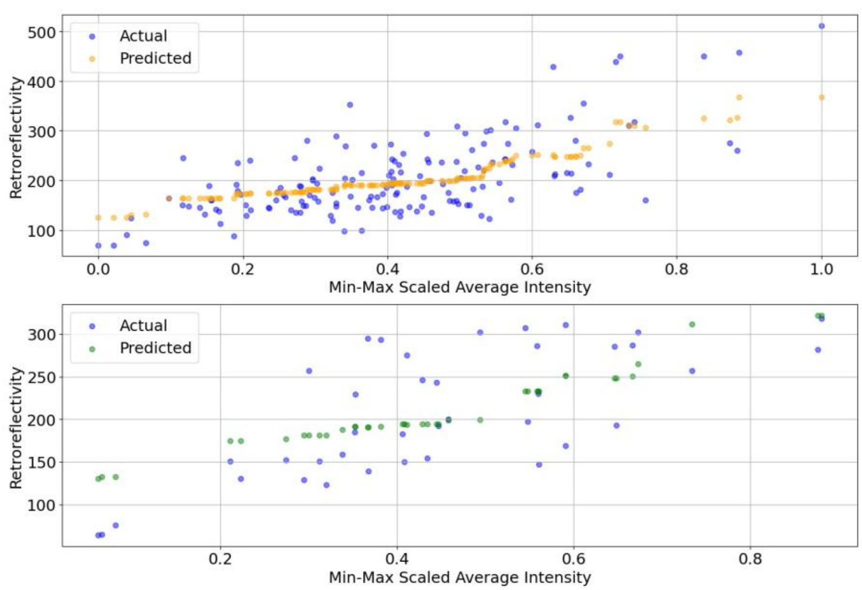

b) I-80 Dashed Line 2 – 3-Lane Sections – Normalized Data and XGBoost Model

Figure 5-31 I-80 Dashed Line 2 – 3-Lane Sections

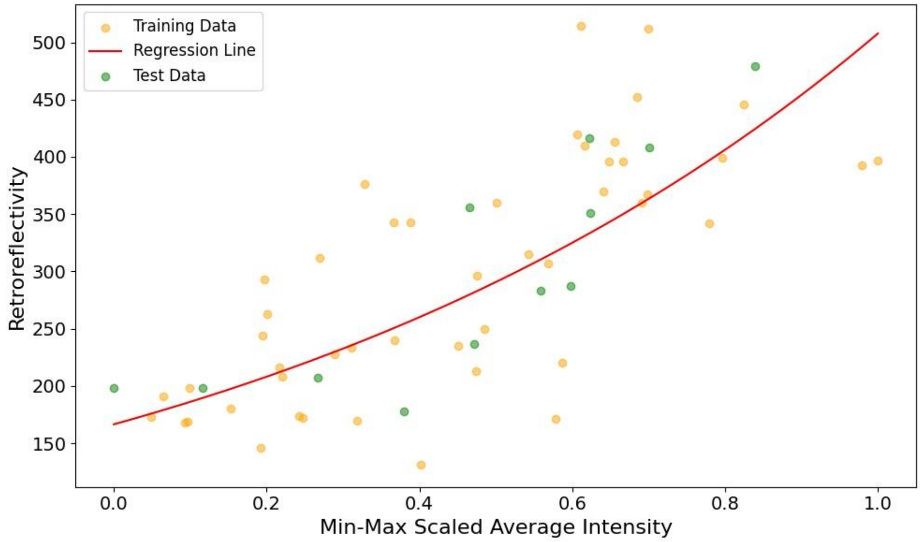

a) I-80 Dashed Line 2 –4-Lane Sections – Normalized Data and Exponential Model

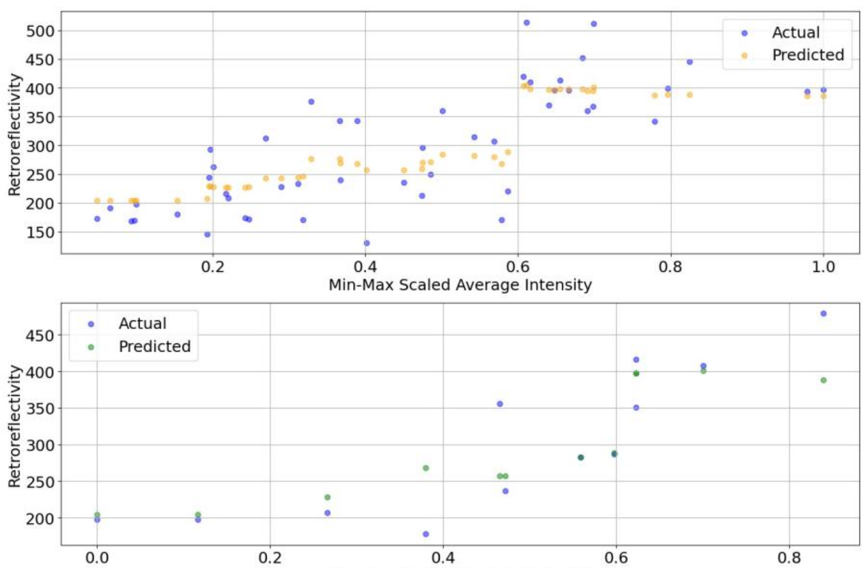

b) I-80 Dashed Line 2 – 4-Lane Sections – Normalized Data and XGBoost Model

Figure 5-32 I-80 Dashed Line 2 – 4-Lane Sections

5.3 Classification Models and Clustering

An essential component of this project is the identification of potential targets for maintenance on the basis of retroreflectivity being estimated below or above a threshold. This is a classification problem and requires different algorithms from those used for regression.

The selected classifier in this research was based on a random forest algorithm. The classifier was defined using a portion of the data for training, and the remaining portion for testing, similar to the process followed above for XGBoost. Typically, a number of iterations of this process are conducted to obtain a more robust approximation of the expected performance of the algorithm, or a cross-validation. So, in this particular case, an 80/20 split was also followed, where 80% of the data was selected for model building, and 20% was selected for model testing. In turn, the cross-validation was performed five times for every model (i.e., a 5-fold cross-validation).

The classification was first evaluated for individual points in terms of the key performance metrics, including accuracy, precision, recall, and F1 score, as shown in Table 5-4. These outcomes were obtained using a similar dataset to that analyzed for the regression analysis, where one point is evaluated every 0.1 miles along the road.

However, such an approach does not take advantage of potential spatial correlations between points close to each other. Pavement marking treatments are expected to be applied to segments of considerable length at a given time, and thus their retroreflectivity should also provide similar performance over the in-service period. Therefore, improvements over these initial classification outcomes were achieved by clustering data points in close proximity to each other.

Clustering was performed as described in section 4.5.1 above, uncovering the expected similarities in retroreflectivity along consistent road segments. Examples of the data sorted by milepost along I-84 for the right and left edge lines in each of the directions of travel are shown in Figures 5-33 and 5-34, where the x-axis shows the mileage along I-84, the y-axis shows the LiDAR intensity, and the colors identify clusters as returned by the algorithm.

Table 5-4 Classification Performance of Random Forest for Different Lanes and Freeways

	Point-Based Classification			
Road Marking	Accuracy	Precision	Recall	F1 Score
I-15 REL NB	0.84	0.94	0.84	0.87
I-15 REL SB	0.74	0.77	0.74	0.75
I-15 LEL NB	0.81	0.82	0.81	0.81
I-15 LEL SB	0.77	0.84	0.77	0.79
I-80 REL EB	0.83	1.00	0.83	0.90
I-80 REL WB	0.76	0.85	0.76	0.80
I-80 LEL EB	0.95	1.00	0.95	0.98
I-80 LEL WB	0.87	0.91	0.87	0.89
I-80 LL EB	0.97	0.94	0.97	0.96
I-80 LL WB	0.82	0.94	0.82	0.88
I-84 REL EB	0.85	0.86	0.85	0.85
I-84 REL WB	0.90	0.90	0.90	0.90
I-84 LEL EB	0.76	0.76	0.76	0.75
I-84 LEL WB	0.74	0.76	0.74	0.75
I-84 LL EB	0.74	0.73	0.74	0.73
I-84 LL WB	0.67	0.68	067	0.67
I-215 REL NB	0.89	0.91	0.89	0.89
I-215 REL SB	0.86	0.86	0.86	0.86
I-215 LEL NB	0.82	0.88	0.82	0.82
I-215 LEL SB	0.83	0.83	0.83	0.83

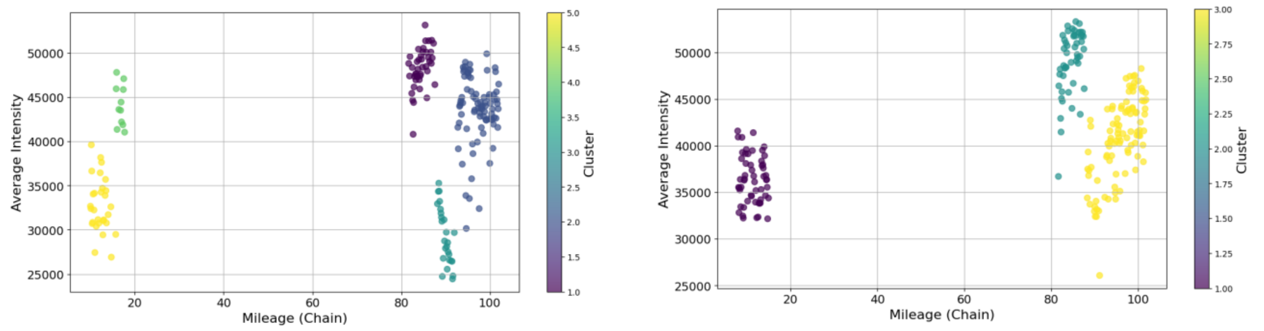

Figure 5-33 Clustering: (a) I-84 Right Edge Line East Bound (b) I-84 Right Edge Line West Bound

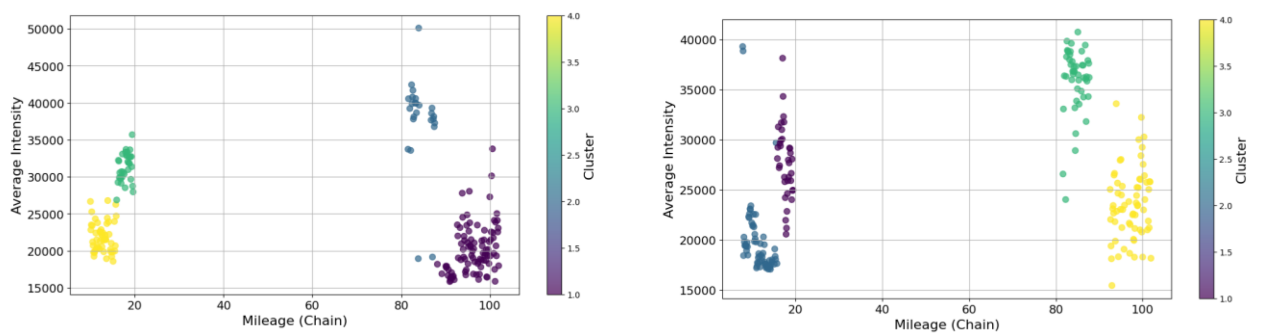

Figure 5-34 Clustering: (a) I-84 Left Edge Line East Bound (b) I-84 Left Edge Line West Bound

It follows that classification outcomes not only using individual points, but rather a consensus from a clustered segment, could reduce variability inherent in short sections.

To do so, each cluster's percentage of points where the retroreflectivity exceeded a minimum threshold (e.g., 100 mcd/m^2/lux) was calculated based on actual values and model predictions. This allowed for assessing the model's accuracy at the segment level, identifying clusters where the model's predictions aligned well with actual measurements and those where discrepancies existed. If the percentage of points above or below the threshold indicates a clear trend in the segment, then high confidence could be assigned to an assessment of the segment as a whole, but some cases may arise when mixed results are obtained, prompting additional point-based attention.

For the data analysis, the following thresholds were applied:

- Segment predicted as "compliant" (i.e., green status): >60% of points located above the threshold.

- Segment predicted as "not compliant" (i.e., red status): <40% of points located above the threshold.

- Segment requiring additional attention (i.e., yellow status): between 40% and 60% of points located above the threshold.

An example of the corresponding visualization for the I-84 data above is shown in Figure 5-35, where segments in each of the directions of traffic for the right and left edge lines can be easily interpreted.

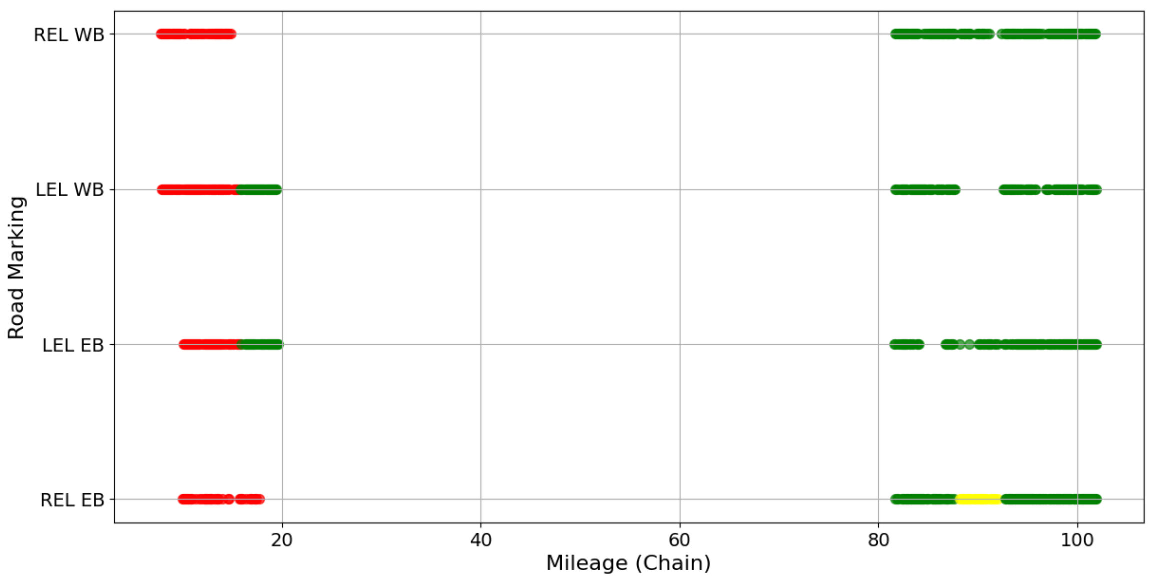

Figure 5-35 Segment-Based Classification for I-84 Using Proposed Thresholds

Moreover, segment-based classification was not only useful for conveying results, but also to improve the overall outcomes across the different key performance measures. This is mainly because localized noise is absorbed by the clusters and generalized together as a single segment trend. A comparison of the classification performance of the point-based and the segment-based setups is shown in Table 5-5.

Table 5-5 Classification Performance of Point-Based and Segment-Based Classification

	Point-Based Classification	Segment-Based Classification
Road Marking	Accuracy	Accuracy
I-15 REL NB	0.84	0.96
I-15 REL SB	0.74	0.96
I-15 LEL NB	0.81	0.95
I-15 LEL SB	0.77	0.93
I-80 REL EB	0.83	1.00
I-80 REL WB	0.76	0.90
I-80 LEL EB	0.95	1.00
I-80 LEL WB	0.87	1.00
I-80 LL EB	0.97	0.95
I-80 LL WB	0.82	1.00
I-84 REL EB	0.85	0.93
I-84 REL WB	0.90	1.00
I-84 LEL EB	0.76	0.97
I-84 LEL WB	0.74	0.87
I-84 LL EB	0.74	0.96
I-84 LL WB	0.67	0.91
I-215 REL NB	0.89	0.89
I-215 REL SB	0.86	0.82
I-215 LEL NB	0.82	1.00
I-215 LEL SB	0.83	1.00

Sample plots of the classification outcomes for the main freeways and lane markings are illustrated below in figures 5-36 through 5-39. From the figures, a close match can be observed between predicted classification outcomes and field-based assessments from the retroreflectivity surveys (labeled as "real cluster" classification). This is true even for smaller models, such as those from I-215, where predictions still provide a reliable source of data for decision-making.

A useful comparison to highlight the benefits of the segment-label classification outcomes would be to contrast the results below with estimations from the regression models in the initial portion of the data analysis. Decisions based on the regression models would be made at the individual point level and would certainly be more difficult to implement along realistic segments. Segment-label classifications are both more reliable and user-friendly, suitable for direct implementation of the methodology proposed in this research.

Figure 5-36 Segment Classification for I-15 – Predicted vs. Field-Based Retroreflectivity

Figure 5-37 Segment Classification for I-80 – Predicted vs. Field-Based Retroreflectivity

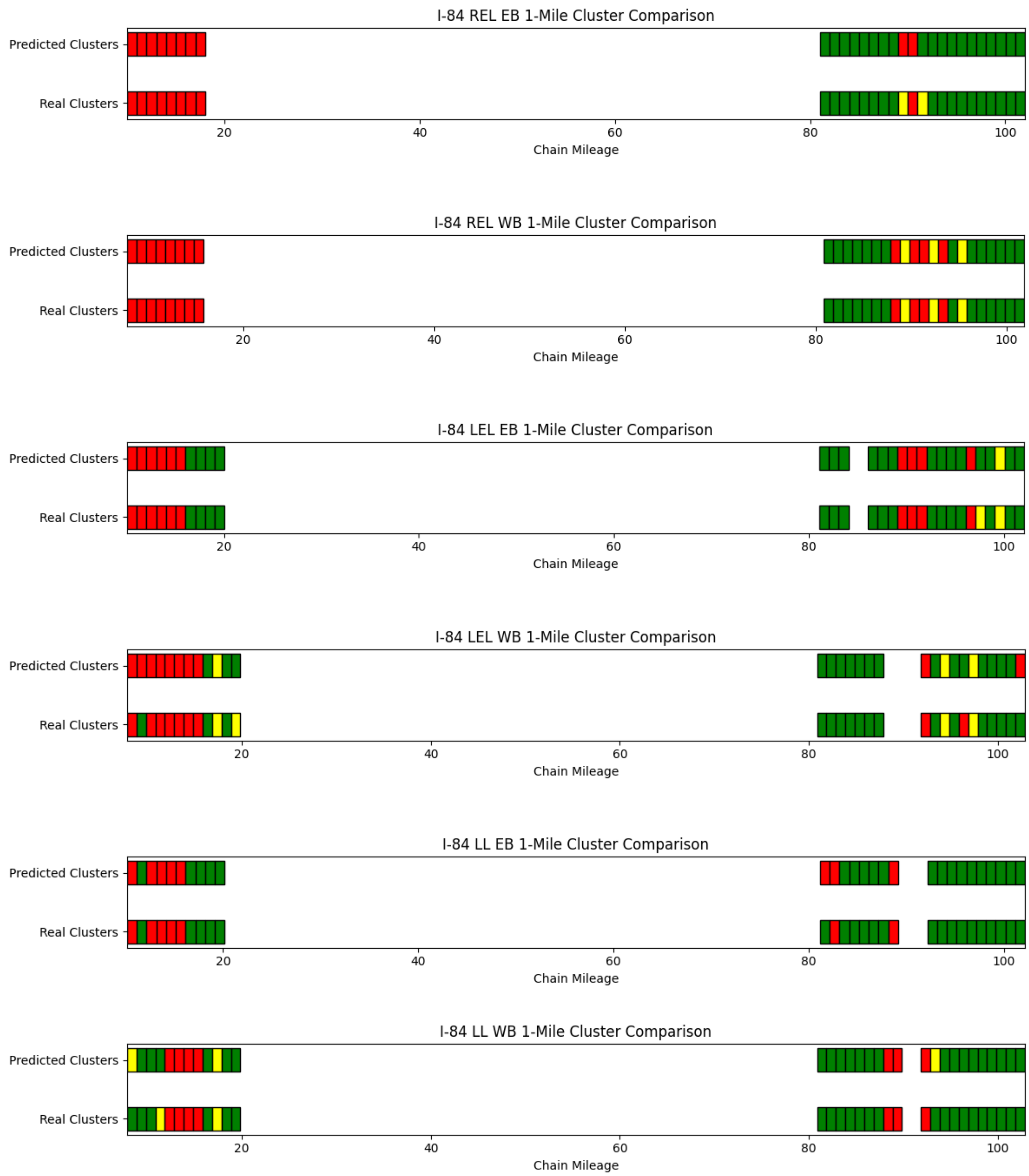

Figure 5-38 Segment Classification for I-84 – Predicted vs. Field-Based Retroreflectivity

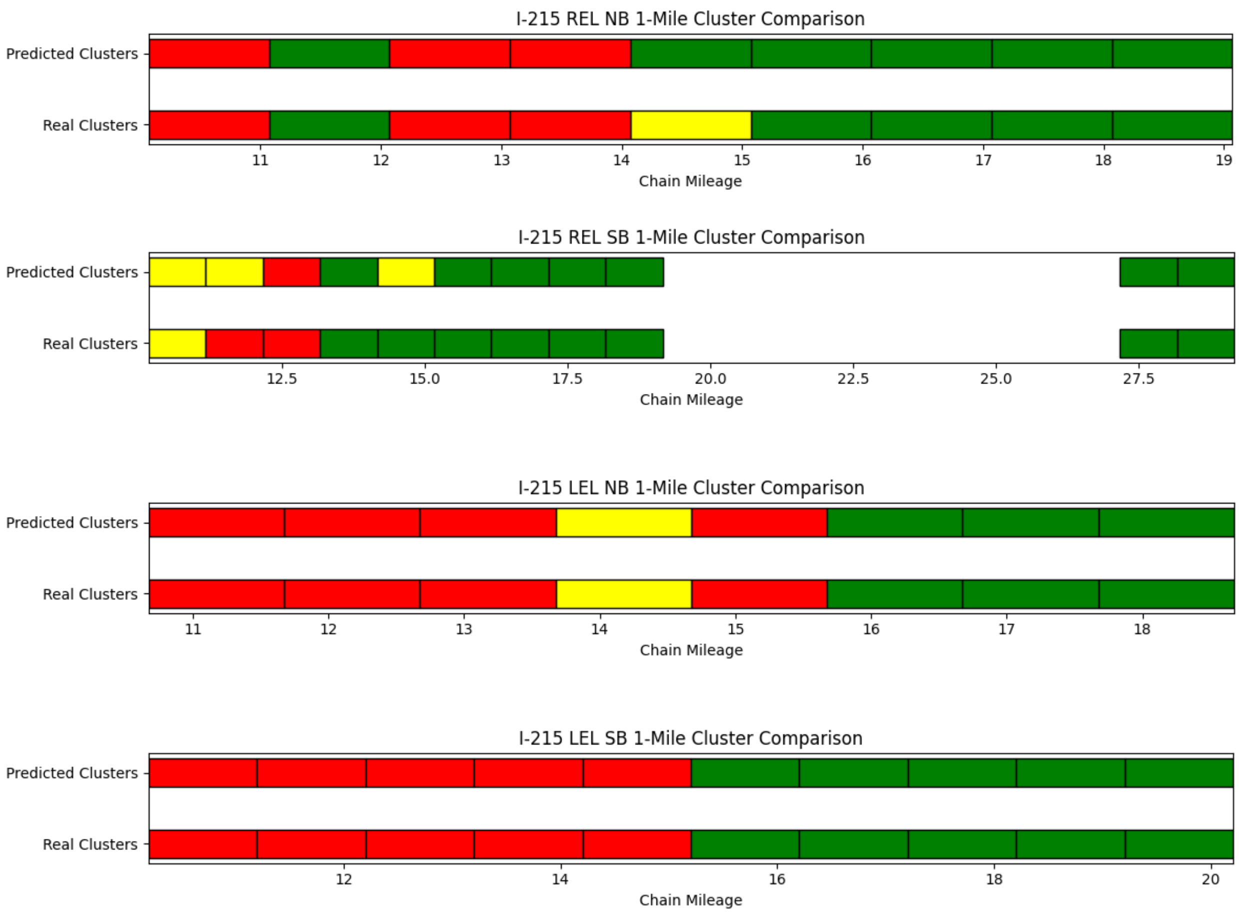

Figure 5-39 Segment Classification for I-84 – Predicted vs. Field-Based Retroreflectivity

6.0 CONCLUSIONS

This research developed a methodology to process LiDAR point cloud data with the objectives of extracting pavement markings and producing reliable retroreflectivity assessments. These efforts demonstrated the feasibility and scalability of the proposed method, resulting in models for estimation and classification. The idea behind leveraging LiDAR data for this purpose stems from an opportunity to reduce reliance on specialized retroreflectometer setups (including mobile setups) to provide inputs and guide maintenance programs that guarantee adequate retroreflectivity levels. Such maintenance programs are essential for traffic safety purposes and, more recently, are also required by FHWA to demonstrate minimum in-service retroreflectivity levels.

Outcomes support the existence of specific associations between retroreflectivity and LiDAR intensity that can be modeled with enough precision to support pavement marking programs. Both exponential regressions and XGBoost-based models can produce R^2 and RMSE values suitable for overall evaluations of retroreflectivity levels and determination of compliance with minimum requirements.

Additional work to cluster individual points adjacent to each other to produce segment-based classification, thereby exploiting potential spatial correlation of retroreflectivity, was also added to the methodology to improve an initial point-based classification process based on random forest algorithms. With the hierarchical clustering algorithm, the models achieve higher accuracy and even approach 100% success for some freeways and line types using 1-mile segment resolutions. This was a significant improvement that provided more stable results and more user-friendly roadway segmentations for practical implementation purposes.

The assessments were obtained for longitudinal pavement markings on freeway segments, including the continuous right and left edge lines, as well as the dashed lane lines, but extensions could also consider other roadway types, further reducing the need for specialized surveys for retroreflectivity measurement.

6.1 Findings

This research provides specific outcomes to support the following overall findings in relation to the objectives of the project:

- Consistent and replicable associations between field-measured retroreflectivity and LiDAR-derived metrics can be modeled for retroreflectivity estimation and classification purposes.

- Specific models for separate lane markings produce satisfactory results despite significantly different angles of data collection and levels of occlusion by other vehicles on the road. Models tested included right edge lines, left edge lines, and lane lines.

- Classification outcomes yield improved performance when individual points are first clustered into segments and then assessed. Such an approach takes advantage of the spatial correlation between nearby points along the freeway and reduces the incidence of localized noise.

- Classification outcomes have high reliability and present a suitable solution for federal reporting needs established by FHWA and required to be in place by September 2026.

6.2 Limitations and Challenges

Significant additional work in this area is still needed to better understand the implications of distance and angle of the marking to the LiDAR sensor, treatment materials, and color, to establish more reliable models to produce high-confidence predictions, particularly at the regression level (not necessarily for classification purposes). Improved regression estimates are essential for more accurate assessments into the future.

In addition, because the available data were drawn primarily from freeway segments with durable pavement markings, the models and thresholds presented here should be interpreted as most representative of durable materials; application to non-durable (short-life) markings would require additional calibration data.

The LiDAR data proved to be consistent and reliable for retroreflectivity estimates, but it can be difficult to work with due to coordinate transformations and high data point resolution. These challenges were addressed via efficient data processing, with the corresponding modeling implications being managed via more flexible algorithms based on machine learning. Particularly, classifiers that take advantage of higher-dimensional spaces have a better chance of resulting in successful models as long as enough field measurements exist for validation and enough LiDAR data is available for training.

7.0 RECOMMENDATIONS AND IMPLEMENTATION

7.1 Recommendations

Outcomes from this research point to specific recommendations in terms of data processing and analysis, where the precise extraction of data from LiDAR point clouds can identify and assess the retroreflectivity or pavement marking with high accuracy. Such pointers can be extracted from the proposed methodology for data processing and analysis.

The research team recommends further testing of prediction and classification outcomes using both the data available for this study and also newly available data from similar locations. This is to enhance the adoption of the proposed methodology and to provide feedback to the researchers for inclusion in the analytical computer tool developed as part of parallel efforts.

In addition, the research team is conducting efforts to expand the outcomes from this project through multi-source assessments that expand the analysis presented here to classifications based not only on LiDAR data but also on street-level imagery, typically collected during the same survey. These assessments are expected to add a new level of reliability to further enhance maintenance decisions.

7.2 Implementation Plan

This project is accompanied by additional efforts to develop a user-friendly implementation tool. This tool is to be provided to UDOT after review by the Technical Advisory Committee and is intended to illustrate the outcomes of the proposed methodology and data analysis, and more importantly, to run analyses using datasets from new LiDAR surveys. Therefore, this tool can provide a clear path for the continuous use of the results of this research in years to come.

The tool is pre-packaged as an executable file that can be ported from one computer to another without the need for external dependencies, so it is a self-contained application. The user is expected to view models and classification outcomes in a format similar to that presented in the results section of this report (including output files for similar tables and figures), with options to view the original models or results of processing new datasets through the existing methodology.

The combination of the outcomes from this research, the multi-source data analysis expansion, and the computer tool (also including a multi-source option) is expected to offer a direct implementation path for UDOT.

REFERENCES

Ai, C., & Hennessy, E. (2022). A pavement marking inventory and retroreflectivity condition assessment method using mobile LiDAR. *Massachusetts Department of Transportation,*.

Barçon, E., Landes, T., Grussenmeyer, P., & Berson, G. (2022). Extraction of road markings from MLS data: a review. 7th International Workshop LowCost 3D-Sensors, Algorithms, Applications 15–16 December 2022, Würzburg, Germany,

Benz, R. J., Pike, A. M., Kuchangi, S. P., & Brackett, Q. (2009a). Mobile retroreflectivity best practices handbook [Tech Report]. https://rosap.ntl.bts.gov/view/dot/16768

Benz, R. J., Pike, A. M., Kuchangi, S. P., & Brackett, Q. (2009b). Serviceable pavement marking retroreflectivity levels : technical report [Tech Report]. https://rosap.ntl.bts.gov/view/dot/16849

Carlson, P. J., Park, E. S., & Andersen, C. K. (2009). Benefits of pavement markings: A renewed perspective based on recent and ongoing research. *Transportation Research Record*, *2107*(1), 59-68.

Che, E., Olsen, M., Parrish, C., & Jung, J. (2019). Pavement Marking Retroreflectivity Estimation and Evaluation using Mobile Lidar Data. *Photogrammetric Engineering & Remote Sensing*, *85*, 573-583. https://doi.org/10.14358/PERS.85.8.573

Chen, H., & Fanny, K. (2019). Understanding the contributing factors to nighttime crashes at freeway mainline segments. *Journal of Transportation Technologies*, *9*(4), 450-461.

Chen, W., Yang, K., Yu, Z., Shi, Y., & Chen, C. P. (2024). A survey on imbalanced learning: latest research, applications and future directions. *Artificial Intelligence Review*, *57*(6), 137.

Cheng, Y.-T., Lin, Y.-C., & Habib, A. (2022). Generalized LiDAR intensity normalization and its positive impact on geometric and learning-based lane marking detection. *Remote Sensing*, *14*(17), 4393.

Cheng, Y.-T., Patel, A., Bullock, D., & Habib, A. (2020). LiDAR-based lane marking extraction through intensity thresholding and deep learning approaches: a pavement-based assessment. *The International Archives of the Photogrammetry, Remote Sensing and Spatial Information Sciences*, *43*, 507-514.

Cheng, Y.-T., Shin, Y.-H., Shin, S.-Y., Koshan, Y., Hodaei, M., Bullock, D., & Habib, A. (2024). Image-aided LiDAR extraction, classification, and characterization of lane markings from mobile mapping data. *Remote Sensing*, *16*(10), 1668.

Federal Highway Administration. (2022). National standards for traffic control devices; the Manual on Uniform Traffic Control Devices for streets and highways; maintaining pavement marking retroreflectivity. *Federal Register*, *87*(150), 47921–47930. https://www.federalregister.gov/documents/2022/08/05/2022-16781/national-standards-for-traffic-control-devices-the-manual-on-uniform-traffic-control-devices-for

Golazad, S., Mohammadi, A., Rashidi, A., & Ilbeigi, M. (2024). From raw to refined: Data preprocessing for construction machine learning (ML), deep learning (DL), and reinforcement learning (RL) models. *Automation in Construction*, *168*, 105844. https://doi.org/https://doi.org/10.1016/j.autcon.2024.105844

Guan, H., Li, J., Cao, S., & Yu, Y. (2016). Use of mobile LiDAR in road information inventory: A review. *International Journal of Image and Data Fusion*, *7*(3), 219-242.

He, H., Xu, A., Han, X., Wang, H., Wang, L., & Su, W. (2023). LiDAR perception and evaluation method for road traffic marking retroreflection. *Transportation Research Record*, *2677*(6), 258-279.

Holzmann, H., & Klar, B. (2024). Robust performance metrics for imbalanced classification problems. *arXiv preprint arXiv:2404.07661*.

Hou, Q., Ai, C., & Boudreau, N. (2024). An automated pavement marking retroreflectivity condition assessment method using mobile LiDAR and video log images. *JOURNAL OF INFRASTRUCTURE SYSTEMS*, *30*(2), 04024004.

Idris, I. I., Mousa, M., & Hassan, M. (2024). Modeling retroreflectivity degradation of pavement markings across the US with advanced machine learning algorithms. *Journal of Infrastructure Preservation and Resilience*, *5*(1), 3.

Kirk, A. R., Hunt, E. A., & Brooks, E. W. (2001). *Factors affecting sign retroreflectivity*.

Kumar, P., McElhinney, C. P., Lewis, P., & McCarthy, T. (2014). Automated road markings extraction from mobile laser scanning data. *International Journal of Applied Earth Observation and Geoinformation*, *32*, 125-137.

Lee, T. (2016). Advanced Methods for Mobile Retro-reflectivity Measurement on Pavement Marking Final Report [Tech Report]. https://rosap.ntl.bts.gov/view/dot/54370

Mahlberg, J. A., Cheng, Y.-T., Bullock, D. M., & Habib, A. (2021). Leveraging LiDAR intensity to evaluate roadway pavement markings. *Future transportation*, *1*(3), 720-736.

Manasreh, D., Nazzal, M. D., & Abbas, A. R. (2024). Feature-Centric Approach for Learning-Based Prediction of Pavement Marking Retroreflectivity from Mobile LiDAR Data. *Buildings*, *14*(1), 62.

Mazzoni, L. N., Vasconcelos, K., Albarracín, O., Bernucci, L., & Linhares, G. (2024). Field data analysis of pavement marking retroreflectivity and its relationship with paint and glass bead characteristics. *Applied Sciences*, *14*(10), 4205.

Migletz, J., & Graham, J. (2002). NCHRP synthesis 306 long-term pavement marking practices. *Transportation Research Board, Washington, DC*.

Migletz, J., Graham, J. L., Bauer, K. M., & Harwood, D. W. (1999). Field Surveys of Pavement-Marking Retroreflectivity. *Transportation Research Record*, *1657*(1), 71-78. https://doi.org/10.3141/1657-10

Mohammadi, A., Golazad, S., & Rashidi, A. (2024). A review of trends and practices in using visual data for construction-related machine learning models. 2024 Winter Simulation Conference (WSC),

Mohammadi, A., Medina, J., & Rashidi, A. Developing a Methodology to Estimate the Retroreflectivity of Longitudinal Pavement Markings using LiDAR.

Mohammadi, A., Medina, J. C., & Rashidi, A. Leveraging Machine Learning and LiDAR for Predictive Maintenance of Roadway Markings. In *Computing in Civil Engineering 2025: Computational and Intelligent Technologies* (pp. 196-205).

Mohammadi, A., Mohammadi, P., Kuang, B., Jiang, G., Rashidi, A., Chen, J., & Wempen, J. (2025). Volumetric Measurement of Salt Piles Using Photogrammetry, LiDAR, and Depth Cameras.

Mousa, M. (2023). Enhanced Decision-Making Framework for the Southern States to Comply with the New Federal Retroreflectivity Pavement Rule.

National Safety Council. (2024). *The most dangerous time to drive*. https://www.nsc.org/road/safety-topics/driving-at-night

Olsen, M. J., Parrish, C., Che, E., Jung, J., & Greenwood, J. (2018). Lidar for maintenance of pavement reflective markings and retroreflective signs. *Oregon Department of Transportation*.

Pike, A. M., Satterfield, C., Schertz, G., Cheung, J., & Falk, K. W. (2022). *Methods for Maintaining Pavement Marking Retroreflectivity* (FHWA-SA-22-028). Federal Highway Administration.

Yang, B., Fang, L., Li, Q., & Li, J. (2012). Automated extraction of road markings from mobile LiDAR point clouds. *Photogrammetric Engineering & Remote Sensing*, *78*(4), 331-338.